SAND REPORT

SAND2009-6425
Unlimited Release
Printed October 2009

Improving electronic structure methods to predict nano-optoelectronics and nano-catalyst functions

Kevin Leung, Ida M.B. Nielsen, John A. Shelnutt, Heather J. Kulik, and Nicola Mazari

Prepared by
Sandia National Laboratories
Albuquerque, New Mexico 87185 and Livermore, California 94550

Sandia is a multiprogram laboratory operated by Sandia Corporation, a Lockheed Martin Company, for the United States Department of Energy under Contract DE-AC04-94AL85000.

Issued by Sandia National Laboratories, operated for the United States Department of Energy by Sandia Corporation.

Available to DOE and DOE contractors from
U.S. Department of Energy
Office of Scientific and Technical Information
P.O. Box 62
Oak Ridge, TN 37831

Telephone:	(865) 576-8401
Facsimile:	(865) 576-5728
E-Mail:	reports@adonis.osti.gov
Online ordering:	http://www.doe.gov/bridge

Available to the public from
U.S. Department of Commerce
National Technical Information Service
5285 Port Royal Rd
Springfield, VA 22161

Telephone:	(800) 553-6847
Facsimile:	(703) 605-6900
E-Mail:	orders@ntis.fedworld.gov
Online ordering:	http://www.ntis.gov/ordering.htm

SAND2009-6425
Unlimited Release
Printed October 2009

Improving electronic structure methods to predict nano-optoelectronics and nano-catalyst functions

Kevin Leung
Surface and Interface Sciences (01114)

Ida M.B. Nielsen
Scalable Computing R & D (08961)

John A. Shelnutt
Ceramic Processing & Inorganic (01815)

Sandia National Laboratories
P.O. Box 5800
Albuquerque, NM 87185

Craig J. Medforth
Department of Chemistry
University of New Mexico

Heather J. Kulik and Nicola Marzari
Department of Materials,
Massachussetts Institute of Technology

Acknowledgement

We thank Nicola Spaldin (UCSB), Gramme Henkelman (UT-Austin) for input, and Ann Mattsson (SNL) for providing the use of the AM05 functional. We also thank Hank Westrich (LDRD office, SNL); NINE organizers Regan Stinnett, Justine Johannes, Duane Dimos, Rene Sells, Glory Emmanuel, Chris Monroe (all SNL); and NINE students Tiffany Hayes (UNM), Zach Pollack (UT-Austin), Elise Li (MIT), and Andrew Paluch (Notre Dame). Finally, we acknowledge the exceptional support by Sandia's high performance computing personnel, including Sophia Corwell, Donna Brown, and others, who have been known to respond to distress calls about supercomputers at 11pm on Saturday nights; the work reported herein would not have been possible without their dedication.

Contents

Figures

Tables

Improving electronic structure methods to predict nano-optoelectronics and nano-catalyst functions

Abstract

This report focuses on quantum chemistry and *ab initio* molecular dynamics (AIMD) calculations applied to elucidate the mechanism of the multi-step, 2-electron, electrochemical reduction of the green house gas molecule carbon dioxide (CO_2) to carbon monoxide (CO) in aqueous media. When combined with H_2 gas to form synthesis ("syn") gas, CO becomes a key precursor to methane, methanol, and other useful hydrocarbon products. To elucidate the mechanism of this reaction, we apply computational electrochemistry which is a fledging, important area of basic science critical to energy storage. This report highlights several approaches, including the calculation of redox potentials, the explicit depiction of liquid water environments using AIMD, and free energy methods. While costly, these pioneering calculations reveal the key role of hydration- and protonation-stablization of reaction intermediates, and may inform the design of CO_2-capture materials as well as its electrochemical reduction. In the course of this work, we have also dealt with the challenges of identifying and applying electronic structure methods which are sufficiently accurate to deal with transition metal ion complex-based catalyst. Such electronic structure methods are also pertinent to the accurate modeling of actinide materials and therefore to nuclear energy research. Our multi-pronged effort towards achieving this titular goal of the LDRD is discussed.

1 General Introduction

The goal of this LDRD project is three-fold. (1) To identify and develop electronic structure computational methods that accurately describe the catalytic, optoelectronic, and electrochemical properties of transition metal ion-based materials, especially those with 1st-row transition metal ions which qualify as "strongly correlated" systems. (2) To apply these methods to model the electrochemical reduction of CO_2 in aqueous solutions. This modeling work is done in parallel with a sister-LDRD (PI: Jim Miller) where most of the experimental work is funded. (3) As part of Sandia's National Institute of Nano Engineering (NINE) program, this LDRD hosts students from NINE partner universities who collaborate on research and participate in summer activities.

Identifying and developing new electronic structure methods

One of the original goals of this LDRD is to identify novel and accurate theoretical methods for predicting the properties of "strongly correlated electron" systems. The test cases used are cobalt porphyrin-catalyzed electrochemical reduction of CO_2 to CO, and solid state CuO properties. Methods we have sampled and tested include quasi-self-interaction-correction (qSIC), self-consistent DFT+U, non-hybrid, semi-local functionals, and quantum chemistry. This effort will be described in Ch. 4.

Electrochemical reduction of CO_2 in water

Photochemical or electrochemical reduction of CO_2 using metal surfaces or organometallic catalysts has been proposed as a method of carbon fixation. The reaction

$$CO_2 + H_2O + 2e^- \rightarrow CO + 2OH^-$$

is a key step in the reverse water-gas shift process to produce syngas (a mixture of CO and H_2) which is the starting material for larger hydrocarbon molecules.

The use of transition metal ion (especially cobalt) based porphyrins, corrins, and other macrocycles to catalyze CO_2 reduction has been pursued by John Shelnutt and coworkers at Sandia. They have applied polymerized cobalt macrocycles layers coated on gas diffusion electrodes. The overall reaction likely takes place in four steps:

$$CoP + CO_2 \rightarrow CoP - CO_2$$

$$\mathrm{CoP} - \mathrm{CO_2} + \mathrm{H^+} \rightarrow \mathrm{CoP} - \mathrm{COOH}$$
$$\mathrm{CoP} - \mathrm{COOH} \rightarrow \mathrm{CoP} - \mathrm{CO} + \mathrm{OH^-}$$
$$\mathrm{CoP} - \mathrm{CO} \rightarrow \mathrm{CoP} + \mathrm{CO}$$

The two electrons can be added to any of the 4 products/intermediates. Thus, the above reaction actually represents 10 different mechanisms depending when electrons are injected.

In this work, we apply Density Functional Theory to study the reaction intermediates of these reactions in water. We seek to address several general issues regarding CoP-catalyzed CO_2 reduction: (1) the difference between aprotic and protic solvents; (2) the optimal charge- and spin-states of the cobalt ion in the intermediates as determined by the electrochemical potentials used in experiments; (3) the energetics of the proposed mechanism, and the determination of whether each step of the multistep reaction goes down hill in free energy; and (4) why high pH conditions facilitates this reaction. Regarding (4): high pH have been found to favor CO production, likely due to a combinbation of catalyst stability, CO_2 solubility, and blockage of the formic acid product channel. However, the CoP-COOH would at first glance seem to be deprotonated at pH=7 or higher. This paradox will be be resolved using DFT and AIMD calculations.

We stress that computational electrochemistry and photoelectrochemistry in general are among the most challenging and timely theoretical chemistry issues today. They are pertinent to modeling electrical energy conversion and storage, photovoltaics, and lithium ion batteries. The challenges of computational electrochemistry are manifold. Accurate modeling of both the solid electrodes and the predominately liquid electrolyes, as well as the interfaces between the two, are required. The liquid state of matter calls for molecular dynamics (or Monte Carlo) techiniques, but the bond-breaking and -making aspects require electronic structure treatments. *Ab initio* molecular dynamics (AIMD) methods methods are ideally suited to this area but are costly to apply. A compromise may be to apply dielectric continuum treatments to approximate the liquid solvent and quantum chemistry techniques to model the reactive regions. This latter approach may be problematic if a metallic electrode is present or if the detailed hydrogen bonding structure strongly affects the reaction mechanism (e.g., when small ions like protons or hydroxides are involved). The catalytic reactions often involve transition metal elements, for which standard DFT methods may not be sufficiently accurate (see above). Electrochemistry studies are conducted at constant potential, not constant number of electrons—which is the default mode of all electronic-structure calculations. Still other challenging aspects, not covered in this report, include long range electron transfer and photochemical reactions. Photon-induced reactions are critical to direct conversion of solar power to chemical energy.

It requires explicit treatment of excited electronic states of molecules and materials, which is inherently difficult. Calculating the rate of long range electron transfer often requires non-adiabatic treatment of electron-solvent/matrix coupling via the Marcus theory. Such issues have received much theoretical interest, but are less critical to CO_2 reduction using porphyrin catalyst. This is because the electron transfer rate may be dominated by engineering issues like the electrical contact between the catalyst and the electrode. In the future, however, both experimental and theoretical methods will be applied to study direct sunlight-induced CO_2 conversion to CO.

The bulk of the quantum chemistry studies will be described in Ch. 2, while Ch. 3 will describe the AIMD studies. These chapters focus on slightly different mechanistic pathways, with the latter using quantum chemistry predicted redox potentials to determine the charge state of each intermediate.

Student activities

Five graduate students participated in the research and NINE educational activities to various extent in this project. Heather Kulik and Elise Li from the Masschussetts Institute of Technology, Tiffany Hayes from the Univerisity of New Mexico, and Andrew Paluch from Notre Dame University all took part in NINE summer student programs. Heather, Tiffany, Andrew, and Zach Pollack from the University of Texas at Austin were actively involved in various research tasks. Heather's work will be briefly described in Ch. 4.

2 Reduction of carbon dioxide by cobalt porphyrins: A density functional study

Introduction

Photochemical or electrochemical reduction of CO_2 using metal or organometallic catalysts has been proposed as a method of carbon fixation. [1, 2, 3] The reaction

$$CO_2 + H_2O + 2e^- \rightarrow CO + 2OH^- \quad (1)$$

is a key step in the reverse water-gas shift process to produce syngas (a mixture of CO and H_2), a starting material for larger hydrocarbon molecules. Large-scale syngas production from CO_2 feedstock in flue gas at room temperature from aqueous solution has recently been proposed.[4] Thermodynamically and electrochemically, the production of CO from Eq. 1 is less favorable than formation of other CO_2 reduction products such as formic acid. However, at high pH and with organometallic, rather than metal, catalysts, the release of CO appears to be kinetically favored.[1, 2, 3] This work applies quantum chemistry calculations to elucidate the reaction intermediates and mechanism in aqueous media.

The use of transition metal ion- (especially cobalt-) based porphyrins, corrins, and other macrocycles to catalyze CO_2 reduction has been extensively studied.[5, 6, 7, 8, 9, 10, 11, 12, 13, 14, 15, 16, 17] Electrochemical, photochemical, and radiolysis reduction routes have been pursued, and binding energies, rate constants, and reactive intermediates have been examined. However, the solvents used in these electrochemical experiments are generally organic solvents. One important conclusion is that, when the catalyst is dispersed in a homogeneous aprotic solvent, or in radiolysis experiments in water, it is activated towards CO_2 after accepting two electrons, i.e., $[CoP]^{2-}$ is involved,[9] where "P" represents a porphyrin moiety, for instance tetraphenylporphyrin.[9] Addition of the first electron to the neutral Co(II)P occurs at -0.7 to -0.9 V relative to the standard hydrogen electrode and generates a $[Co(I)P]^-$ species. Addition of a second electron occurs at ~ -2.0 V, and can either yield a Co(0)P species or a reduction of the porphyrin ring.[10] Thus, a substantial, negative electrochemical potential, the precise value of which depends on the solvent and the porphyrin substituents, is needed to reduce CO_2.

Recently, high yield reduction of CO_2 to CO in aqueous media at a more economical, < -0.8 V, electrochemical potential has been demonstrated.[18, 19, 20, 21, 22, 23, 24, 25] These processes apply stable polymerized cobalt macrocycles coated on gas diffusion electrodes. The relatively low electrochemical potential, which are

only 0.2-0.3 volt more negative than the redox potential of Co(I)P/Co(II)P couple in water, suggests that the Co(I)P charge state of the catalyst is sufficient to reduce CO_2 to CO.[23, 24] The two initial steps in the carbon dioxide reduction are likely to involve the formation of a complex between the porphyrin and carbon dioxide followed by addition of a proton[1]; assuming that the starting point is $[CoP]^{n-}$, the first two steps will then be

$$[CoP]^{n-} + CO_2 \rightarrow [CoP\text{–}CO_2]^{n-} \tag{2}$$

$$[CoP\text{-}CO]_2^{n-} + H^+ \rightarrow [CoP\text{–}COOH]^{(n-1)-} \tag{3}$$

Subsequently, the reaction then proceeds to form $CoP\text{–}CO^{(n-1)-}$ and eventually CoP. The reduction mechanism for CO_2 reduction in water, however, is not as well studied as the reduction in aprotic solvents. In particular, the detailed charge- and spin states of the various X-ligated intermediates, where "X" can be CO, CO_2, or COOH, have not been elucidated. As the electrochemical potentials of [Co(I)P-X]/[Co(II)P-X] and [Co(0)P-X]/[Co(I)P-X] couples depend on X, it is not clear where the two electrons required to reduce CO_2 to CO are added.

After formation of CoP–COOH, the next step may be a reduction followed by decomposition to either H_2O and CO or to HCOOH:

$$[CoP\text{–}COOH]^{(n-1)-} + e^- \rightarrow [CoP\text{–}COOH]^{n-} \tag{4}$$

$$[CoP\text{–}COOH]^{n-} + H^+ \rightarrow CoP^{(n-1)-} + CO + H_2O \tag{5}$$

$$[CoP\text{–}COOH]^{n-} + H^+ \rightarrow CoP^{(n-1)-} + HCOOH \tag{6}$$

Alternatively, protonation of CoP–COOH may lead to a decomposition, forming $[CoP\text{-}CO]^{(n-2)}-$, followed by a reduction that causes dissociation into CoP and CO

$$[CoP\text{–}COOH]^{(n-1)-} + H^+ \rightarrow [CoP\text{–}CO]^{(n-2)-} + H_2O \tag{7}$$

$$[CoP\text{–}CO]^{(n-2)-} + e^- \rightarrow [CoP]^{(n-1)-} + CO \tag{8}$$

Finally, the cycle may be completed by reduction of the formed neutral cobalt porphine

$$CoP^{(n-1)-} + e^- \rightarrow [CoP]^{n-} \tag{9}$$

In this work, we apply Density Functional Theory to study the energetics of the reaction steps proposed in the reduction of CO_2 catalyzed by cobalt porphyrin in water. We will focus on charge states that reflect $n = 1$ but will also explore alternative n values. In the various reactions modeled, we will use the cobalt porphyrin with the simplest porphyrin unit, namely porphine. The investigation focuses on determining the free energies in aqueous solution for the various proposed reaction

intermediates, while reaction rates and activation barriers will be deferred to a future study. Although our work is specific to cobalt porphyrin-catalyzed CO_2 reduction, the insights obtained will enhance understanding of such electrochemical reactions using organometallic catalysts in water, which have so far received little theoretical attention. Specific issues to be addressed here include determination of the structure and spin multiplicity of the electronic ground state for all porphyrin species involved; comparison of energetics obtained with hybrid (B3LYP) and pure (PBE and BP86) functionals; and computation of solvation free energies and thermal corrections to determine total reaction free energies in aqueous solution at 298.15 K for the proposed steps in the reduction of carbon dioxide by cobalt porphyrins.

Theoretical Methods

Geometries were optimized with the B3LYP[26, 27] (and in a several cases PBE[28]) density functional method. For open-shell species, the unrestricted variants were used, and for all species investigated, the stability of the wave function was checked (using the stable=opt option in Gaussian03), to detect UHF or other instabilities and ensure that the lowest energy solution was obtained. The geometry optimizations for neutral species and cations employed a 6-31G* basis set[29, 30, 31, 32], which is a valence double-ζ set augmented with a single set of polarization functions on all atoms except hydrogen. For anions, geometries were optimized using the 6-31+G* basis[33], which is derived from the 6-31G* basis by addition of a set of diffuse functions on all non-hydrogen atoms. The nature of all located stationary points was established by computation of harmonic vibrational frequencies, and, unless otherwise noted, every stationary point was found to be a minimum. At the optimized geometries, single point energies were also computed with the 6-31+G* basis for all species. Additionally, for comparison with B3LYP results, single point energies were computed with the 6-31+G* basis using the PBE and BP86[34, 35] functionals. Solvent effects were addressed by computation of single point energies using the polarizable continuum (PCM) model at the B3LYP/6-31+G* level of theory (using the default molecular cavity in Gaussian03) with water as the solvent. Unless otherwise noted, geometry optimizations were performed in the gas phase; to investigate the solvent effect on the geometry, a few geometry optimizations were also performed using the PCM model with water as the solvent. To establish the binding energy for $[CoP–CO]^+$, single point energies were also computed with the B3LYP, PBE, and BP86 methods using the 6-311++G(2d,2p) basis[36, 37, 33, 38, 39]; these computations were carried out both in the gas phase and in solution, using water and CH_2Cl_2 as solvents. All computations were performed with the Gaussian03 program package[40].

Structures and Spin Multiplicities for Cobalt Porphyrin Intermediates

To select an appropriate level of theory for geometry optimizations, we first optimized the structure of the neutral (doublet) cobalt tetraphenylporphyrin molecule (CoTPP) whose structure has been determined by X-ray diffraction[41]. We used the B3LYP and PBE methods and the 6-31G* basis. Both the computed and experimental structures have S_4 symmetry, and the computed bond distances are in good agreement with experiment, with the B3LYP method performing slightly better. The B3LYP and PBE Co−N bond distances were found to be 1.962 and 1.930 Å, respectively, in reasonable agreement with the experimental value of 1.949 Å; the computed C−N and C−C bond distances are all in good agreement with experimental bond distances, with the B3LYP values being within about 0.005 Å of these. The B3LYP method has also been found to yield a geometry in good agreement with experiment for nickel porphine when used with the 6-31G* basis (and using Ahlrichs' VTZ basis on Ni).[42] On the basis of these results, we chose to perform B3LYP optimizations using the 6-31G* basis. Since inclusion of diffuse functions may be important for anions, however, the 6-31+G* basis was employed in all optimizations for anionic species.

All open-shell species were optimized using unrestricted wave functions, and all closed-shell singlets were checked for UHF instabilities. Unless otherwise indicated, all singlets were found to be pure singlets ($\langle S^2\rangle$=0.0), whereas there is some spin contamination in the triplet states ($\langle S^2\rangle$ around 2.2−2.5). For doublet-quartet systems, the spin contamination in both the doublet and quartet states is essentially negligible.

$[CoP]^-$, CoP, and $[CoP]^+$

We first consider cobalt porphine without any ligands. A schematic of cobalt porphine, labeling the different atom types, is shown in Fig. 1. For the neutral CoP we optimized a doublet and quartet state, and for both of the charged species $[CoP]^+$ and $[CoP]^-$, we optimized singlet and triplet states. For $[CoP]^+$, the ground state is found to be a triplet, whereas the ground states for CoP and $[CoP]^-$ are the low-spin configurations, a doublet and a singlet state, respectively.

We find the ground state of CoP to be a $^2A_{1g}$ state; this is also the ground state for cobalt tetraphenylporphyrin, as determined by analysis of ESR data[43]. We found the lowest quartet state, a $^4B_{1g}$ state, to be 8.8 kcal mol^{-1} above the ground state (determined from single-point B3LYP/6-31+G* energies at optimum B3LYP/6-31G* geometries). Both the doublet and quartet states are minima, planar with D_{4h}

symmetry. Thus, both states have delocalized π bonds so that, within each structure, all N$-$C$_\alpha$ bond distances are equal, as are all C$_\alpha-$C$_m$ and C$_\alpha-$C$_\beta$ distances. The main differences in the geometries for the two structures are found for the Co$-$N distances, which assume values of 1.978 and 2.036 Å in the doublet and quartet, respectively, and for the C$_\alpha-$C$_m$ distances, which are 1.382 Å in the doublet and 1.395 Å in the quartet.

The optimum B3LYP/6-31G* ground state geometry for $[CoP]^+$ is a nonplanar $^3B_2$ structure with D_{2d} symmetry. In this structure the porphyrin ring is ruffled, with the planes of opposite pyrrole rings twisted in opposite directions (as shown in Fig. 2); the ruffling angle, γ(C$_\alpha$-N-N-C$_\alpha$) (see Fig. 1) is 16.2°. The structure has delocalized π bonds so that all C$_\alpha-$C$_\beta$ bond distances are identical, and likewise for all C$_\alpha-$C$_m$ and N$-$C$_\alpha$ bonds; the Co$-$N bond distance is found to be 1.947 Å. A search for a singlet structure (using an unrestricted wave function) yielded a spin-broken state with $\langle S^2\rangle = 1.0$, which is a transition state and lies 3.8 kcal mol^{-1} above the triplet ground state. For $[CoP]^+$ there is also a low-lying quintet state with C_{4h} symmetry, which is 5.2 kcal mol^{-1} above the ground state. Because the B3LYP method tends to favor high-spin states over low-spin states (see Section 2), and hence may favor a triplet, rather than a singlet, ground state, we also performed geometry optimizations for $[CoP]^+$ using the PBE method. With the PBE method, minima were located for both the singlet and triplet states, and the triplet state was found to be the ground state, 9.2 kcal mol^{-1} below the singlet.

For $[CoP]^-$, the ground state is a singlet state with C_{2h} symmetry. This is a pure singlet, although there is a spin-broken state with $\langle S^2\rangle = 0.8$, which, at the same geometry, is about 3 kcal mol^{-1} lower in energy. In the following, energies reported for $[CoP]^-$ will pertain to the pure singlet state. On the triplet surface, a minimum was located, a $^3A'$ state with C_s symmetry, and it lies 15.9 kcal mol^{-1} above the singlet minimum. With an $\langle S^2\rangle$ value of 2.5, this triplet state has a significant amount of spin contamination; at this geometry, however, a check for instabilities in the wave function yields another, even more spin-contaminated, $^3A'$ state ($\langle S^2\rangle = 2.8$) that lies only about 1 kcal mol^{-1} above the (pure) singlet minimum.

Considering the ground state geometries for the neutral and charged cobalt porphines, the Co$-$N distance increases as electrons are added. Thus, the Co$-$N distance in the ground state configurations of $[CoP]^+$, CoP, and $[CoP]^-$ are 1.947, 1.978, and 1.980 Å, respectively. While CoP and $[CoP]^-$ are planar, the porphine ring in $[CoP]^+$ is slightly ruffled with a γ(C$_\alpha$-N-N-C$_\alpha$) angle of 16.2 degrees. The observed ruffling of the ring for smaller metal-nitrogen distances is consistent with previous findings for nickel porphyrins[44] demonstrating that a shortening of the metal-nitrogen distance is accompanied by a ruffling of the ring, with nonplanarity setting in for distances be-

low ca. 1.95 Å. Note that the significant lengthening of the Co−N bond distance upon addition of electrons was not found in a previous DFT study[45], which computed Co−N bond distances of 1.988 and 1.991 Å for CoP^+ and CoP, respectively.

Other Intermediates

In addition to the neutral and charged naked cobalt porphine, the intermediates in the proposed CO_2 reduction mechanism include cobalt porphine with various ligands: $[CoP–COO]^-$, $[CoP–COO]^{2-}$, CoP–COOH, $[CoP–COOH]^-$, and $[CoP–CO]^+$. B3LYP/6-31G* (and B3LYP/6-31+G* for anions) geometry optimizations for the lowest electronic states for these species yielded low-spin ground states in all cases, namely a singlet for $[CoP–COO]^-$, CoP–COOH, and $[CoP–CO]^+$ and a doublet for $[CoP–COOH]^-$ and $[CoP–COO]^{2-}$. The optimized ground state structures are shown in Fig. 2. The singlet states are all pure singlets, and the doublet state is slightly spin-contaminated ($\langle S^2 \rangle = 0.77$ and 0.79 for $[CoP–COOH]^-$ and $[CoP–COO]^{2-}$, respectively). For the singlet states, the largest singlet-triplet energy difference is found for CoP–COOH, for which the lowest-lying triplet state is 19.9 kcal mol^{-1} above the ground state, whereas the located triplet states for $[CoP–COO]^-$ and $[CoP–CO]^+$ are only 6.8 and 6.3 kcal mol^{-1}, respectively, above the singlet ground states. Additionally, a low-lying quartet state 3.8 kcal mol^{-1} above the doublet ground state was located for $[CoP–COOH]^-$.

For singlet CoP–COOH, a B3LYP/6-31G* geometry optimization was also performed using the PCM solvation model with water as the solvent. The aqueous-phase geometry is very similar to the optimum gas-phase geometry (although inclusion of diffuse functions in the basis set could possibly yield more significant differences). Both structures have a planar porphyrin ring with the COOH ligand oriented as illustrated in Fig. 2, and inclusion of solvation effects has an insignificant effect on the porphyrin ring, which has nearly the same Co–N distance in the gas phase and in water (1.986 Å on the OH side and 1.978 Å on the opposite side). The largest changes in the geometry upon inclusion of solvent effects are a lengthening of the Co–C bond distance from 1.884 to 1.889 Å and a shortening of the C=O and C–OH bond distances from 1.209 and 1.359 Å to 1.200 and 1.355 Å.

An optimization in the aqueous phase was also carried out for the singlet anion $[CoP–COO]^-$ using the B3LYP/6-31+G* level of theory. Again, inclusion of solvation effects leaves the ring geometry nearly unchanged, but there is a substantial shortening of the Co–C bond distance; the gas-phase Co–C bond distance is 1.2.192 Å, and this bond shortens to 1.986 Å in aqueous solution. The optimum C–O bond distances also

change somewhat, increasing from 1.213 Å in the gas phase to 1.245 Å in solution, and the C–O–C angle contracts from 143.9 to 131.0 degrees.

Charge and Spin on Co Atom

Using a Mulliken population analysis (based on the B3LYP wave function with the 6-31G* basis, or 6-31+G* for anions), the atomic charge on the cobalt atom in the porphine species was computed, and the results are shown in Table 1. In the neutral and positivily charged porphines, the net charge on Co in both the ground and excited states was found to be nearly 1 (ranging from 0.80 to 1.08). In the singly charged anions, the Co atom is nearly neutral (charges ranging from −0.39 to −0.07) in the ground state, which is always low-spin, whereas the Co charge in $[\text{CoP-COO}]^{2-}$ is −0.81; in the excited states, the Co charge varies considerably, assuming values of −1.46, −1.09, and 0.16 for for triplet $[\text{CoP-COO}]^{-}$, quartet $[\text{CoP-COOH}]^{-}$, and triplet $[\text{CoP}]^{-}$, respectively.

The total Mulliken spin densities on the Co atom are also listed in Table 1. In the (restricted) singlet states, the spin density is always zero. In the open-shell species, a doublet has a total spin density (summed over all atoms) of 1; for a triplet, the total spin density is 2, and so on. Considering the spin density on Co in the open-shell species, we note that it is nearly equal to the overall spin density of the molecule for most species, with a few exceptions: For triplet $[\text{CoP-CO}]^{+}$ and doublet $[\text{CoP-COOH}]^{-}$ and $[\text{CoP-COO}]^{2-}$, the Co spin density assumes values of 0.99, 0.00, and 0.17, respectively, and, hence, in these species there is an unpaired electron on the porphyrin ring; the same is the case for the open-shell singlet (transition state) located for $[\text{CoP}]^{+}$, which has a spin density of 1.16 on Co.

Binding energy for $[\text{CoP–CO}]^{+}$

The cationic complex $[\text{CoP–CO}]^{+}$ is one of the intermediates in the proposed mechanism for reduction of CO_2 by cobalt porphine (Eqs. 7 and 8). Perhaps just as significantly, this species yield an important benchmark test for the theoretical methods used. While experimental work[46] has shown that Co(II) does not bind CO, the binding of CO to the cobalt tetraphenylporphyrin cation $[\text{CoTPP}]^{+}$, a cobalt porphyrin involving Co(III), has been demonstrated experimentally. Thus, electrooxidation of CoTPP in CH_2Cl_2[46] yielded $\log K = 4.3$, where K is the formation constant at 300 K for the reaction

$$[\text{CoTPP}]^{+} + \text{CO} \rightleftharpoons [\text{CoTPP–CO}]^{+}. \tag{10}$$

From this result, a binding free energy $\Delta G^{300}_{\rm bind} = 5.9$ kcal mol^{-1} for binding of CO to [CoTPP]$^+$ in CH_2Cl_2 at 300 K is obtained. Note that the experimental work employed a standard state concentration of 1.0 M in both the gas phase and in solution; these values were derived from thermodynamic cycle arguments, and thus the spin of the reactants and products are not conserved.

We are not aware of any experimental data on the binding energy of [CoP–CO]$^+$, however, and we here investigate the stability of this complex, determining the free energy for binding of CO to [CoP]$^+$ by considering the reaction

$$[\text{CoP–CO}]^+ \rightarrow [\text{CoP}]^+ + \text{CO} \tag{11}$$

with all species in their ground electronic state (viz., singlet states for [CoP–CO]$^+$ and CO and a triplet state for [CoP]$^+$). Our results are shown in Table 2, which details the individual contributions to the binding energy, including zero-point vibrational energy, thermal corrections, and solvation free energies. Computations were performed in the gas phase as well as in water and CH_2Cl_2 using the B3LYP, PBE, and BP86 methods with the 6-311++G(2df,2pd) basis set. Optimum geometries, zero-point energies, and thermal corrections were determined with both B3LYP and PBE using the 6-31G* basis (the BP86 energies were computed at the B3LYP geometries). Note that the solvation calculations by default employ a concentration of 1 atm in the gas phase and 1 M in solution; to compare our data with experimental results using a 1 M standard state concentration throughout, we therefore convert to a 1 M concentration in the gas phase by applying a correction of +1.89 kcal mol^{-1} to the gas-phase reaction free energy

The total B3LYP binding free energy, $\Delta G^{298.15}_{\rm bind}$, is predicted to be negative, assuming values of -5.0 kcal mol^{-1} in water and -5.5 kcal mol^{-1} in CH_2Cl_2. The gas-phase binding energy at 0 K, $\Delta E^0_{\rm bind,(g)}$, is 10.2 kcal mol^{-1}, and inclusion of zero-point vibrational energy (-2.4 kcal mol^{-1}) and solvation (-3.8 kcal mol^{-1} in H_2O and -4.4 kcal mol^{-1} in CH_2Cl_2) yields binding free energies at 0 K, $\Delta G^0_{\rm bind}$, of 4.0 and 3.4 kcal mol^{-1} in H_2O and CH_2Cl_2, respectively. The thermal correction is sizeable, however (-10.8 kcal mol^{-1}), resulting in negative finite-temperature binding free energies $\Delta G^{298.15}_{\rm bind}$; the thermal correction is the sum of a small enthalpy correction of +0.6 kcal mol^{-1} and a large entropy term, $-TS = -11.4$ kcal mol^{-1}. The entropy contribution to the binding energy is similar to values reported previously[47] in a study of the binding of nitric oxide to Fe-hemes, which found an entropic contribution to the binding free energy at 298 K of -13.5 kcal mol^{-1} (from theory) and -8.72 kcal mol^{-1} (from experiment). The B3LYP method has previously been found to yield poor agreement with experiment for Co–C bonds energies in tetrapyrroles and similar systems because it fails to provide a consistent treatment of correlation energies for

transition metal complexes with different numbers of unpaired electrons,[48]; also the B3LYP method is known to favor high-spin states relative to low-spin states beacuse of inclusion of Fermi correlation in the Hartree-Fock exchange.[49]. It is therefore likely that the reaction energy for Eq. 11 predicted by B3LYP will be too small.

The PBE method, however, predicts a considerably more stable complex, and the binding free energy in solution at finite temperature is $\Delta G^{298.15}_{\rm bind} = 16.2$ kcal mol^{-1} obtained in CH_2Cl_2. While the zero-temperature gas-phase PBE binding energy of 29.2 kcal mol^{-1} is significantly larger than its B3LYP counterpart (10.2 kcal mol^{-1}), the other contributions to $\Delta G^{298.15}_{\rm bind}$ are similar at the PBE and B3LYP levels. Thus, the B3LYP and PBE zero-point vibrational energies and thermal corrections are nearly identical, differing by only 0.2 kcal mol^{-1}, although there is a somewhat larger, 1.5 kcal mol^{-1}, difference in the solvation contributions. The BP86 results are similar to the PBE values, with a zero-temperature gas-phase BP86 binding energy, $\Delta E^{0}_{\rm bind,(g)} = 27.4$ kcal mol^{-1} and a solvation contribution $\Delta G_{\rm solv}$ of -2.2 kcal mol^{-1}.

Our B3LYP value of -5.5 kcal mol^{-1} for $\Delta G^{298.15}_{\rm bind}$ for [CoP–CO]$^+$ in CH_2Cl_2 and the corresponding PBE and BP86 values of 16.2 and 13.9 kcal mol^{-1}, respectively, bracket the experimental value of 5.9 kcal mol^{-1} for $\Delta G^{300}_{\rm bind}$ for [CoTPP–CO]$^+$. The binding energies for [CoP–CO]$^+$ and [CoTPP–CO]$^+$ will probably differ somewhat, because the phenyl rings perturb the porphyrin ring a little. Thus the porphyrin ring is found to contract slightly upon addition of phenyl groups as evidenced by the Co–N bond distances of 1.977 and 1.963 Å predicted for the ground states of CoP and CoTPP, respectively, at the B3LYP/6-31G* level of theory. However, the phenyl rings most likely will not significantly affect the charges on N and Co, and probably will have only a small effect on the binding of CO. Our preliminary calculations using the plane-wave basis VASP code (see the next chapter) shows that the binding energy between Co(III)P and CO, and that between Co(III)TPP and CO, differ only by 1.5 kcal/mol. Our B3LYP and BP86 predictions are consistent with results[45] obtained for the binding of nitric oxide to [CoP]$^+$ showing the B3LYP method to underestimate and the BP86 method to overestimate the binding energy relative to an experimentally determined binding energy for [CoTPP–NO]$^+$.

Finally, we also investigated the effect of optimizing geometries in solution, rather than in the gas phase. For singlet [CoP-CO]$^+$, a B3LYP/6-31G* geometry optimization in aqueous solution lowered the energy by only 0.2 kcal mol^{-1} relative to the energy obtained by a single point solvation calculation at the gas-phase geometry. Thus, we expect optimization in solution to have a very small effect on the computed reaction energy for Eq. 11.

Reaction Energies and Free Energies for Proposed Steps

The reaction energies for the proposed steps in the reduction of CO_2 by cobalt porphine, Eqs. 2–9, are listed in Table 3. The spin multiplicities for the porphine species that appear in the reactions are also given in Table 3. For the porphine species, structures were optimized for both the low-spin and intermediate-spin states, and, as discussed in Section 2, the low-spin form was found to be the ground state in all cases except $[CoP]^+$, which has a triplet ground state. Determination of aqueous-phase reaction free energies $\Delta G_{aq}^{298.15}$ entailed computation of gas-phase free energies $G_g^{298.15}$ for all species to which were added the computed solvation free energies (see Table 3 for details), and these computations were all performed at the B3LYP/6-31+G* level of theory. The hydration free energy of the proton is required to compute the reaction free energies in aqueous solution for several of these reactions, and we have employed a value from the literature, $\Delta G_{hyd.}^{298}(H^+) = -262.4$ kcal mol^{-1}, predicted by high-level *ab initio* electronic structure methods.[50] Total gas-phase energies, zero-point vibrational energies, thermal corrections, and free energies of solvation employed to compute the reaction energies in Table 3 are given in the Supporting Information. As mentioned in Section 2, failure to provide consistent treatment of electron correlation in transition metal complexes with different numbers of unpaired electrons is a potential shortcoming of the B3LYP method,[48, 49] and we may expect the reactions involving a change of spin for the porphine species to be difficult cases for B3LYP. We therefore also computed gas-phase reaction energies using the pure functionals PBE and BP86, and the resulting energies are given in Table 3 as well.

Considering the gas-phase reaction energies, we find that B3LYP differs significantly from PBE and BP86 for all reactions in which the spin of the porphine changes, but not for other reactions. For reactions in which the spin multiplicity of the porphine increases (Eqs. 4 and 8), the B3LYP reaction energy is substantially lower than the PBE and BP86 energies; when the spin multiplicity of the porphine decreases, however, (Eq. 9), the B3LYP reaction energy is much higher than the PBE and BP86 values. For reactions that do not involve a change of spin multiplicity, there is good agreement between B3LYP and BP86, with an average absolute error of 2.8 kcal mol^{-1} and a maximum discrepancy of 5.3 kcal mol^{-1}. The agreement between B3LYP and PBE is not quite as good, with average absolute and maximum errors of 5.1 kcal mol^{-1} and 9.5 kcal mol^{-1}, respectively. For all reactions, regardless of the spin multiplicities involved, the PBE and BP86 results are similar, with an average absolute deviation of 2.6 kcal mol^{-1} and a maximum error of 5.9 kcal mol^{-1}, and the BP86 method yields lower reaction energies in most cases.

The tendency of the B3LYP method to lower the energy of a high-spin state

relative to that of a low-spin state could possible affect its ability to predict the correct spin multiplicity for the ground state[49]. With one exception, however, all of the porphyrin species considered were found to have a low-spin ground state, so this tendency does not seem to have affected the ordering of states, although we might expect the singlet-triplet and doublet-quartet splittings predicted by B3LYP to be too small. In one case the B3LYP method does predict a high-spin ground state, finding a triplet ground state for $[CoP]^+$, but in this case the PBE method predicts a triplet ground state as well (which is 9.2 kcal mol^{-1} below the singlet). While geometries were optimized in the gas phase, inclusion of solvation energies (computed at the optimum gas-phase geometries) did not change the ordering of the states except for $[CoP{-}COOH]^-$, for which inclusion of solvation brings the total free energy in solution (at 298 K) of the quartet state nearly 5 kcal mol^{-1} below the doublet. The PBE and BP86 methods, however, find the doublet state to be significantly below the quartet, and the energies reported in Table 3 therefore pertain to the doublet state of $[CoP{-}COOH]^-$. We note, that a density functional study of a number of iron (Fe(II) and Fe(III)) complexes with low- intermediate-, or high-spin ground states (previously established by experiment) found the B3LYP method (and several other hybrid functionals) to predict the correct spin multiplicy for the ground state for all complexes[51], although B3LYP appears to be incorrect in predicting a low-spin ground state for iron porphyrin difluoride.[52]

From the aqueous-phase reaction energies in Table 3, we can evaluate the proposed reaction mechanism in terms of the energetics for each reaction step. In the aqueous phase, two reactions, Eqs. 2 and 7, are somewhat endothermic, whereas all other reactions are exothermic. For Eqs. 2 and 7, the three density functional methods are in good agreement; given the small differences in the ΔE_g^0 values predicted by B3LYP, PBE, and BP86 for these reactions, and the similarity in solvation and thermal corrections obtained with B3LYP and PBE (see Section 2), the $\Delta G_{aq}^{298.15}$ value would probably be positive with all three methods. Considering Eq. 7, performing optimizations in the aqueous phase, instead of the gas phase as done here, should cause only negligible changes in the reaction energy. Thus, we showed in Section 2 that geometry optimization in the aqueous phase lowers the energy of $[CoP\text{-}CO]^+$ by only 0.2 kcal mol^{-1}. Therefore, we believe Eq. 7 to be endothermic, especially at experimental pH values of 7 or above, and, hence, this step is not likely to be part of the CO_2 reaction mechanism. $CoPCOOH^-$ is a more likely intermediate via Eq. 5. For Eq. 2, aqueous-phase optimization at the B3LYP/6-31+G* level for $[CoP\text{-}COO]^-$ lowers the aqueous phase energy by 4.4 kcal mol^{-1} relative to the aqueous-phase energy computed at the optimum gas-phase geometry, whereas aqueous-phase geometry optimization for $[CoP]^-$ lowers the energy by only 0.1 kcal mol^{-1}. Thus, using aqueous-phase geometries would lower the reaction free energy $\Delta G_{aq}^{298.15}$ by about 4.3

kcal mol^{-1}, yielding a B3LYP value of $\Delta G_{\mathrm{aq}}^{298.15} = 3.3$ kcal mol^{-1}. The PBE and BP86 gas-phase reaction energies for this reaction are a few kcal mol^{-1} lower than the B3LYP value; Eq. 2 thus appears to be nearly thermoneutral and could be a possible reaction step. The inclusion of explicit water molecules in the model may render this reaction even more favorable. On the other hand,

$$[\mathrm{CoP}]^{2-} + \mathrm{CO_2} \rightarrow [\mathrm{CoP–CO}]_2^{2-} \tag{12}$$

is far more exothermic and favorable. This reaction involves CoP-$CO_2{}^{2-}$, which may be formed via a simultaneous addition of CO_2 and e^-. CoP-$CO_2{}^{2-}$ is known to present in aprotic solvents. In the future, we will explore this reaction route.

On the basis of these results, we conclude that all but one of the proposed reaction steps, Eqs. 2–9 are viable intermediate steps in the CO_2 reduction mechanism, and only Eq. 7, can be ruled out. In the next chapter, we further make use of redox potential calculations to ascertain when electrons are added to the system.

Concluding Remarks

We have investigated the aqueous-phase reduction of carbon dioxide by cobalt porphine using density functional theory, including the B3LYP, PBE, and BP86 methods. Optimum structures and harmonic vibrational frequencies were determined for low-lying electronic states of cobalt porphines that are potential intermediates in the reduction mechanism. Both planar and non-planar cobalt porphine structures were located; a non-planar, ruffled structure was found for the ground state of $[\mathrm{CoP}]^+$, which has the smallest Co–N distance (1.947 Å) of the porphine species investigated. The differences between reaction energies computed with the B3LYP, PBE, and BP86 methods were investigated; generally, the methods agree well for isogyric reactions, but large discrepancies between the hybrid (B3LYP) and pure (PBE and BP86) methods were found for reactions in which the spin multiplicity of the porphine species changes. The gas-phase and solution-phase (H_2O and CH_2Cl_2) energies for binding of CO to cobalt porphine were determined and comparison with experimental data reveals that the B3LYP method most likely underestimates, while the PBE and BP86 methods overestimate, the binding energy. Aqueous-phase reaction free energies were obtained for all proposed intermediate steps in the carbon dioxide reduction mechanism, and most of the steps were found to be exothermic; in particular, the mechanism is likely to involve a $[\mathrm{CoP\text{-}COO}]^{2-}$ intermediate, which may be formed with simultaneous addition of CO_2 and e^- to CoP^-. The reaction between [CoP–COOH] and a proton, forming $[\mathrm{CoP\text{-}CO}]^+$ and H_2O, was found to be endothermic, however,

and hence an unlikely intermediate step in the mechanism; instead, $[\text{CoP–COOH}]^-$, obtained from protonation of $[\text{CoP-COO}]^{2-}$, is a more likely intermediate.

Table 1. Mulliken charges and atomic spin densities on the Co atom[a]

[a] Computed from the B3LYP wave function using a 6-31G* basis (6-31+G* for anions). For each species, the ground state is listed first. [b] This is a transition state (and is an open-shell singlet with with $\langle S^2 \rangle = 1.05$).

	Charge	Spin
CoP (doublet)	0.96	1.15
CoP (quartet)	0.96	2.76
$[CoP]^+$ (triplet)	1.07	1.91
$[CoP]^+$ (singlet)	1.01	1.16
$[CoP]^-$ (singlet)	−0.07	0.00
$[CoP]^-$ (triplet)	0.16	2.33
$[CoP\text{-}CO]^{+,b}$ (singlet)	0.87	0.00
$[CoP\text{-}CO]^+$ (triplet)	0.88	0.99
$[CoP\text{-}COO]^-$ (singlet)	−0.33	0.00
$[CoP\text{-}COO]^-$ (triplet)	−1.46	2.31
$[CoP\text{-}COO]^{2-}$ (doublet)	−0.81	0.17
[CoP-COOH] (singlet)	0.80	0.00
[CoP-COOH] (triplet)	0.91	2.35
$[CoP\text{-}COOH]^-$ (doublet)	−0.39	0.00
$[CoP\text{-}COOH]^-$ (quartet)	−1.10	2.78

Table 2. Contributions (kcal mol^{-1}) to the total binding energy[a], $\Delta G^{298.15}_{\rm bind}$, for [CoP–CO]$^+$ in the aqueous phase and in CH_2Cl_2.

	B3LYP		PBE	BP86
	H_2O	CH_2Cl_2	CH_2Cl_2	CH_2Cl_2
$\Delta E^{0}_{\rm bind,(g)}$ [b]	10.17	10.17	29.18	27.40
Δ ZPVE[c]	−2.39	−2.39	−2.55	−2.55[g]
$\Delta G^{c,d}_{\rm thermal}$	−10.79	−10.79	−10.61	−10.61[g]
$\Delta G^{e}_{\rm solv}$	−3.83	−4.37	−1.69	− 2.22
Standard state conversion[f]	+1.89	+1.89	+1.89	+ 1.89
$\Delta G^{298.15}_{\rm bind}$	−4.95	−5.49	16.22	13.91

[a] Using a 1 M reference state both in solution and in the gas phase.
[b] 6-311++G(2d,2p) value at 0 K in the gas phase.
[c] 6-31G* value in the gas phase.
[d] Computed as $\Delta G^{298.15}_{\rm bind,g.} - \Delta G^{0}_{\rm bind,g}$.
[e] 6-311++G(2d,2p) value computed in H_2O or CH_2Cl_2.
[f] Conversion from 1 atm to 1 M standard state in the gas phase.
[g] Using the PBE value.

Table 3. Reaction energies (kcal mol^{-1}) for proposed steps in the reduction of CO_2 by cobalt porphyrins; reduction potentials (eV) given in parentheses. After each porphyrin species the spin multiplicity is given in parentheses, with 1=singlet, 2=doublet, etc.[a]

Eq.		$\Delta G_{aq}^{298.15}$ B3LYP	ΔE_g^0 B3LYP	ΔE_g^0 PBE	ΔE_g^0 BP86
(2)	$[CoP]^-(1) + CO_2 \rightarrow [CoP–CO_2]^-(1)$	7.63	0.38	−3.73	−1.70
(3)	$[CoP–CO_2]^-(1) + H^+ \rightarrow CoP–COOH(1)$	−10.39	−327.71	−321.57	−322.42
(4)	$CoP–COOH(1) + e^- \rightarrow [CoP–COOH]^-(2)$	−75.30 (−1.17)	−30.32	−8.10	−9.92
(5)	$[CoP–COOH]^-(2) + H^+ \rightarrow CoP(2) + CO + H_2O$	−48.69	−338.88	−329.39	−335.30
(6)	$[CoP–COOH]^-(2) + H^+ \rightarrow CoP(2) + HCOOH$	−56.17	−352.06	−349.58	−352.98
(7)	$CoP–COOH(1) + H^+ \rightarrow [CoP–CO]^+(1) + H_2O$	5.10	−221.19	−218.01	−221.75
(8)	$[CoP–CO]^+(1) + e^- \rightarrow CoP(2) + CO$	−129.09 (−1.16)	−148.01	−119.48	−123.46
(9)	$CoP(2) + e^- \rightarrow [CoP]^-(1)$	−63.02 (−1.71)	−24.73	−43.46	−45.48
(12)	$[CoP–COO]^{2-}(2) + H^+ \rightarrow [CoP\text{-}COOH]^-(2)$	−18.92	−406.58	−401.44	−402.41

[a] ΔE_g^0 is the gas-phase reaction energy at 0 K computed with a 6-31+G* basis set. In all cases, employed geometries were optimized at the B3LYP level with the 6-31+G* (for anions) or 6-31G* basis. $\Delta G_{aq}^{298.15}$ represents the reaction free energy in aqueous solution at 298.15 K computed using the B3LYP/6-31+G* ΔE_g^0 value, converting to $\Delta G_g^{298.15}$ by adding ZPVE and thermal corrections, and adding the free energy of solvation computed at the B3LYP/6-31+G* level. Note that the reaction free energies are listed for pH=0 conditions; to convert to pH=7 (close to pH of many of the aqueous media electrochemical work cited[18, 19, 20, 21, 22, 23, 24, 25]), 9.6 kcal/mol should be added—which would make Eq. 3 almost thermoneutral. The reduction potentials are referenced to the normal hydrogen electrode with the reaction $\frac{1}{2}H_2 \rightarrow e^- + H^+(aq)$, employing an absolute potential of 4.44 V[53].

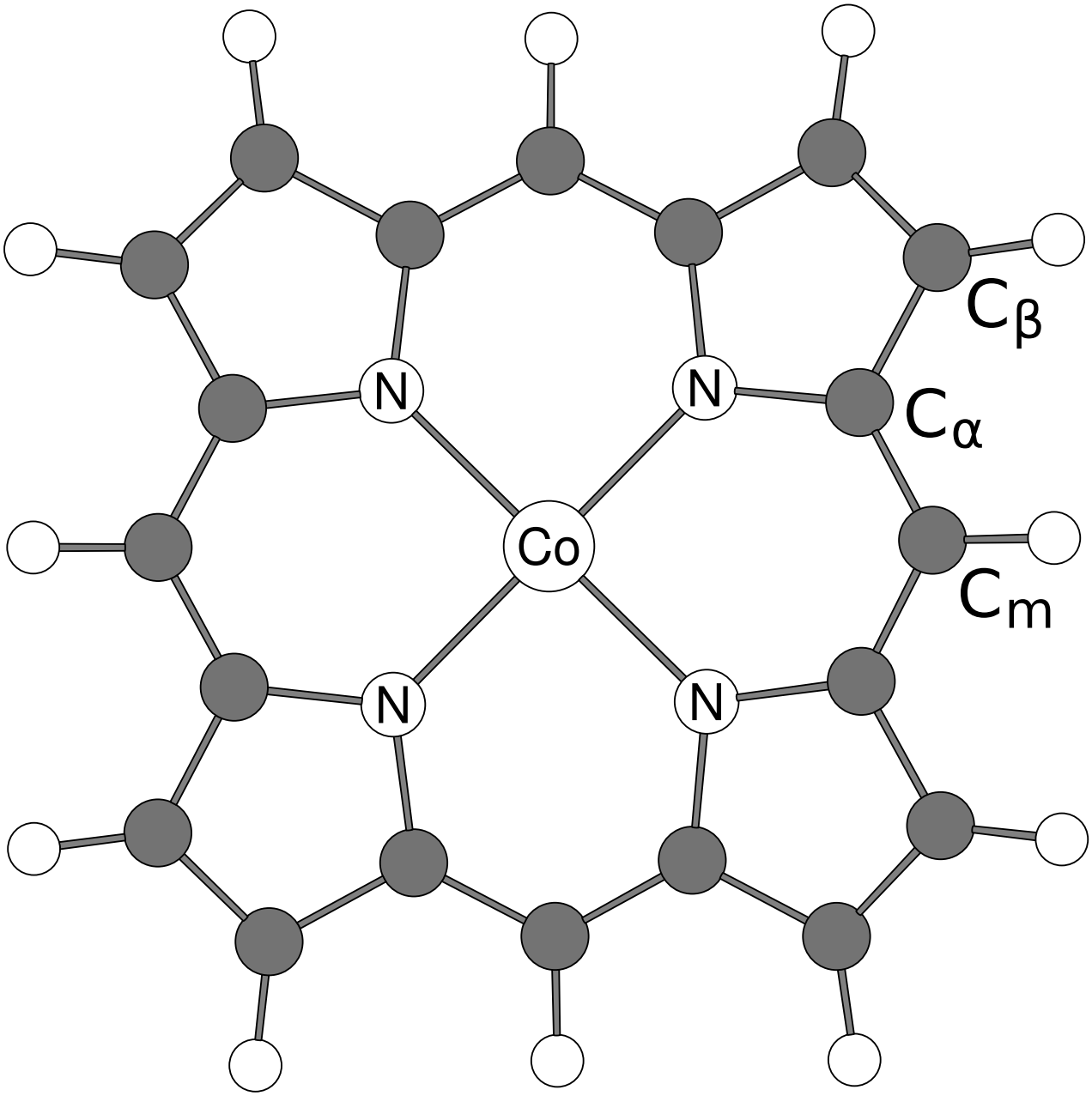

Figure 1. Cobalt porphine with different types of carbon atoms identified.

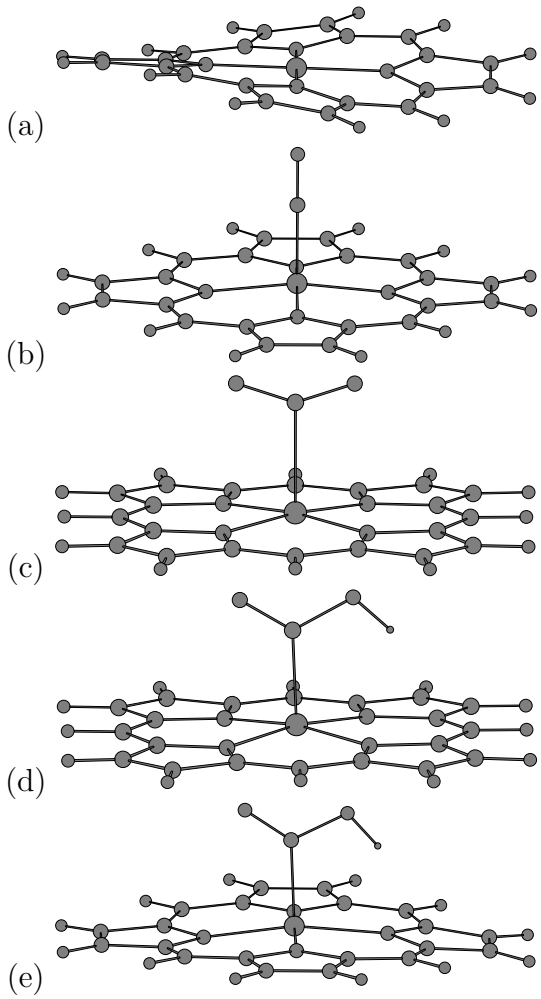

Figure 2. B3LYP optimum ground state structures for cobalt porphines: (a) $[CoP]^+$; (b) $[CoP–CO]^+$; (c) $[CoP–COO]^-$; (d) CoP–COOH; (e) $[CoP–COOH]^-$. Note that the porphyrin ring in (c), (d), and (e) is oriented so that the COO or COOH moiety is parallel to the plane of the page. The porphyrin ring is planar in (b), (c), and (d), and nearly planar in (e), while the ruffled porphyrin ring in (a) displays greater deviation from planarity. The ground state structure of $[CoP-COO]^{2-}$ (not shown) is similar to that of $[CoP–COO]^-$.

References

[1] Arakawa, H.; Aresta, M.; Armor, J.N.; Barteau, M.A.; Beckman, E.J.; Bell, A.T.; Bercaw, J.E.; Creutz, C.; Dinjus, E.; Dixon, D.A.; Domen, K.; DuBois, D.L.; Eckert, J.; Fujita, E.; Gibson, D.H.; Goddard, W.A.; Goodman, D.W.; Keller, J.; Kubas, G.J.; Kung, H.H.; Lyon, J.E.; Manzer, L.E.; Marks, T.J.; Morokuma, K.; Nicolas, K.M.; Periana, R.; Que, L.; Rostrup-Nielson J.; Sachtler, W.M.W.; Schmidt, L.D.; Sen, A.; Somorjai, G.A.; Stair, P.C.; Stults, R.; Tumas, W. *Chem. Rev.* **2001**, *101*, 953.

[2] Chaplin R.P.S.; Wragg, A.A.; *J. Appl. Electrochem.* **2003**, *33*, 1107.

[3] Fujita, E. *Coord. Chem. Rev.* **1999**, *185*, 373.

[4] Delacourt, C.; Ridgway, P.L.; Kerr, J.B.; Newman, J. *J. Electrochem. Soc.* **2008**, *155*, B42.

[5] Grodkowski, J.; Neta, P.; Fujita, E.; Mahammed, A.; Simkhovich, L.; Gross, Z. *J. Phys. Chem. A* **2002**, *106*, 4772.

[6] Grodkowski J.; Neta, P. *J. Phys. Chem. A* **2000**, *104*, 4475.

[7] Grodkowski J.; Neta, P. *J. Phys. Chem. A* **2000**, *104*, 1848.

[8] Grodkowski, J.; Dhanaeskaran, T.; Neta, P.; Hambright, P.; Brunschwig, B.S.; Shinozaki, K.; Fujita, E. *J. Phys. Chem. A* **2000**, *104*, 11332.

[9] Dhanasekaran, T.; Grodkowski, J.; Neta, P.; Hambright, P.; Fujita, E. *J. Phys. Chem. A* **1999**, *103*, 7742.

[10] Behar, E.; Dhanasekaran, T.; Neta, P.; Hosten, C.M.; Ejeh, D.; Hambright, P.; Fujita, E. *J. Phys. Chem. A* **1998**, *102*, 2870.

[11] Fujita, E.; Furenlid, L.R.; Renner, M.W. *J. Am. Chem. Soc.* **1997**, *119*, 4549.

[12] Ogata, T.; Yanagida, S.; Brunschwig, B.S.; Fujita, E. *J. Am. Chem. Soc.* **1995**, **117**, 6708.

[13] Fujita, E.; Creutz, C.; Sutin, N.; Brunschwig, B.S. *Inorg. Chem.* **1993**, **32**, 2657.

[14] Matsuoka, S.; Yamamoto, K.; Ogata, T.; Kusaba, M.; Nakashima, N.; Fujita, E.; Yanagida, S. *J. Am. Chem. Soc.* **1993**, *115*, 601.

[15] Creutz, C.; Schwarz, H.A.; Wishart, J.S.; Fujita, E.; Sutin, N. *J. Am. Chem. Soc.* **1991**, *113*, 3361.

[16] Fujita, E.; Creutz, C.; Sutin, N.; Szalda, D.J. *J. Am. Chem. Soc.* **1991**, *113*, 343.

[17] Creutz, C.; Schwarz, H.A.; Wishart, J.F.; Fujita, E.; Sutin, N. *J. Am. Chem. Soc.* **1989**, *111*, 1153.

[18] Magdesieva, T.V.; Butin, K.P.; Yamamoto, T.; Tryk, D.A.; Fujishima, A. *J. Electrochem. Soc.* **2003**, *150*, E608.

[19] Magdesieva, T.V.; Yamamoto, T.; Tryk, D.A.; Fujishima, A. *J. Electrochem. Soc.* **2002**, *149*, D89.

[20] Sonoyama, N.; Kirii, M; Sakata, T. *Electrochem. Commun.* **1999**, *1*, 213.

[21] Ramirez, G.; Ferraudi, G.; Chen. Y.-Y.; Trollund, E.; Villagra, D. *Inorg. Chim. Acta* **2009**, **362**, 5.

[22] Ramirez, G.; Lucero, M.; Riquelme, A.; Villagran, M.; Costamagna, J.; Trollund, E.; Aguirre, M.J. *J. Coord. Chem.* **2004**, *57*, 249.

[23] Dreyse, P.; Ramirez, G.; Riquelme, A.; Isaacs, M. *J. Chil. Chem. Soc.* **2006**, *51*, 923.

[24] Riquelme, M.A.; Isaacs, M.; Lucero, M.; Trollund, E.; Aguirre, M.J. *J. Chil. Chem. Soc.* **2003**, *49*, 2.

[25] Ryba, G.; Shelnutt, J.; Prarie, M.R.; Assink, R.A. *Sandia SAND report* **1997**, *97*-0414.

[26] Becke A.D. *J. Chem. Phys.*, **1993**, *98*, 5648.

[27] Lee, C.T.; Yang, W.T.; Parr, R G. *Phys. Rev. B* **1988**, *37*, 785.

[28] Perdew J.P.; Burke K.; Ernzerhof M. *Phys. Rev. Lett.* **1996**, *77*, 3865.

[29] Ditchfield, R.; Hehre, W.J.; Pople, J.A. *J. Chem. Phys.* **1971**, *54*, 724

[30] Hehre, W.J.; Ditchfield, R.; Pople, J.A. *J. Chem .Phys.* **1972**, *56*, 2257.

[31] Hariharan, P.C.; Pople, J.A. *Theor. Chim. Acta* **1973**, *28*, 213.

[32] Rassolov, V.A.; Pople, J.A. ; Ratner, M.A.; Windus, T.L. *J. Chem. Phys.* **1998**, *109*, 1223.

[33] Clark, T.; Chandrasekhar, J.; Spitznagel, G.W.; v. R. Schleyer, P. *J. Comp. Chem.* **1983**, *3*, 294.

[34] Perdew. J.P. *Phys. Rev. B* **1986**, *33*, 8822.

[35] Becke, A.D. *Phys. Rev. A* **1998**, *38*, 3098.

[36] Krishnan, R.; Binkley, J.S.; Seeger, R.; Pople, J.A. *J. Chem. Phys.* **1980**, *72*, 650.

[37] Frisch, M.J.; Pople, J.A.; Binkley, J.S. *J. Chem. Phys.* **1984**, *80*, 3265.

[38] Wachters, A.J.H. *J. Chem. Phys.* **1970**, *52*, 1033.

[39] Hay, P.J. *J. Chem. Phys.* **1977**, *66*, 4377.

[40] Gaussian 03, Revision E.01, Frisch, M. J.; Trucks, G. W.; Schlegel, H. B.; Scuseria, G. E.; Robb, M. A.; Cheeseman, J. R.; Montgomery Jr., J. A.; Vreven, T.; Kudin, K. N.; Burant, J. C.; Millam, J. M.; Iyengar, S. S.; Tomasi, J.; Barone, V.;, Mennucci, B.; Cossi, M.; Scalmani, G.; Rega, N.; Petersson, G. A.; Nakatsuji, H.; Hada, M.; Ehara, M.; Toyota, K.; Fukuda, R.; Hasegawa, J.; Ishida, M.; Nakajima, T.; Honda, Y.; Kitao, O.; Nakai, H.; Klene, M.; Li, X.; Knox, J. E.; Hratchian, H. P.; Cross, J.B.; Adamo, C.; Jaramillo, J.; Gomperts, R.; Stratmann, R. E.; Yazyev, O.; Austin, A. J.; Cammi, R.; Pomelli, C.; Ochterski, J. W.; Ayala, P. Y.; Morokuma, K.; Voth, G. A.; Salvador, P.; Dannenberg, J. J.; Zakrzewski, V. G.; Dapprich, S.; Daniels, A. D.; Strain, M. C.; Farkas, O.; Malick, D. K.; Rabuck, A. D.; Raghavachari, K.; Foresman, J. B.; Ortiz, J. V.; Cui, Q.; Baboul, A. G.; Clifford, S.; Cioslowski, J.; Stefanov, B. B.; Liu, G.; Liashenko, A.; Piskorz, P.; Komaromi, I.; Martin, R. L.; Fox, D. J.; Keith, T.; Al-Laham, A. A.; Peng, C. Y.; Nanayakkara, A.; Challacombe, M.;, Gill, P. M. W.; Johnson, B.; Chen, W.; Wong, M. W.; Gonzalez, C.; Pople, J. A. Gaussian, Inc. (Wallingford CT, 2004)

[41] Madura, P.; Scheidt, W.R. *Inorg. Chem.* **1976**, *15*, 3182.

[42] Kozlowski, P.M.; Rush III, T.S.; Jarzecki, A.A.; Zgierski, M.Z. Chase, B.; Piffat, C.; Ye, B.-H.; Li, X.-Y.; Pulay, P.; Spiro, T.G.. *J. Phys. Chem. A* **1999**, *103*, 1357.

[43] Lin, W.C. *Inorg. Chem.* **1976**, *15*, 1114.

[44] Song, Y.J.; Haddad, R.E.; Jia, S.-L.; Hok, S.; Olmstead, M.M.; Nurco, D.J.; Schore, N.E.; Zhang, J.; Ma, J.-G.; Smith, K.M.; Gazeau, S.; Pécaut, J.; Marchon, J.C.; Medforth, C.J.; Shelnutt, J.A. *J. Am. Chem. Soc.* **2005**, *127*, 1179.

[45] Jaworska, M. *Chem. Phys.* **2007**, *332*, 203.

[46] Mu, X.H.; Kadish, K.M. *Inorg. Chem.* **1989**, *28*, 3743.

[47] Chiavarino, B.; Crestoni, M.E.; Fornarini, S.; Rovira, C. *Inorg. Chem.* **2008**, *47*, 7792.

[48] Jensen, K.P.; Ryde, U. *J. Phys. Chem. A* **2003**, *107*, 7539.

[49] Reiher, M.; Salomon, O.; Hess, B.A. *Theor. Chem. Acc.* **2001**, *107*, 48.

[50] Zhan, C.-G.; Dixon, D.A. *J. Phys. Chem. A* **2001**, *105*, 11534.

[51] Swart, M.; Groenhof, A.R.; Ehlers, A.W.; Lammerstma, K. *J. Phys. Chem. A* **2004**, *108*, 5479.

[52] Ghosh, A.; Taylor, P.R. *J. Chem. Theor. Comp.* **2005**, *1*, 597.

[53] Trasatti, S. *Pure Appl. Chem.* **1986**, *58*, 955.

3 Redox potentials, pK_a, and C-OH cleavage barrier of key intermediates

Introduction

In this chapter, we use a combination of quantum chemistry and *ab initio* molecular dynamics (AIMD) techniques to examine further details of the $CO_2 + 2\ e^- \rightarrow CO$ mechanism. First we extract redox potentials from quantum chemistry calculations, which determine when the two electrons are added. Then we focus on AIMD simulations of the protonation of CO_2, critical to the reduction of the carbon atom from the +4 to the +2 oxidation state and removal of an oxygen atom. This answers the question why protonation proceeds despite the fact that the pH in the experimental conditions range from pH=7 to 12 while -COOH carboxylate acid groups are generally deprotonated at pH < 5. We also consider the activation barrier associated with the breaking of the C-OH bond to release CO.

Method

Details of the quantum chemistry calculations are described in the previous chapter. AIMD simulations apply the VASP code,[1, 2] the Perdew-Burke-Ernzerhof (PBE) functional,[3] Γ-point Brillouin zone sampling, 400 eV planewave energy cutoff, deuterium masses for all protons to allow Born-Oppenheimer dynamics time steps of 0.25 fs, a 10^{-6} eV energy convergence criterion, and T=425 K NVT conditions. At T=400 K, the PBE functional yields water structure consistent with experimentally observed water $g(r)$ at T=300 K.[4] We raise the temperature by an extra 25 K to ensure better sampling statistics.

As described in Ch. 1, semi-local functionals such as PBE are generally inadequate for treating first row transition metal ions such as cobalt. In fact, Ch. 2 shows that two widely used functionals, PBE and B3LYP (the latter a hybrid), predict values for the binding energy of the following reaction,

$$[\mathrm{Co(III)P}]^+ + \mathrm{CO} \rightarrow [\mathrm{Co(III)P - CO}]^+, \tag{13}$$

which differ from the experimental value by ~ 0.5 eV in opposite directions. Therefore we apply the DFT+U method[5] to the partially occupied d-orbitals of the Co ion. DFT+U have been successfully used to model transition metal porphyrin complexes adsorbed on metal electrodes and dispersed in water.[6, 7], Using the VASP code

reduced	oxidized	B3LYP	PBE	DFT+U
$Co(I)P^{-}$	Co(II)P	-1.7	-0.9	-1.5
$Co(I)P^{2-}$	$Co(I)P^{-}$	-2.1	-2.3	NA
$CoP(I){CO_2}^{2-}$	$Co(I)PCO_2^{-}$	-1.7	NA	-1.6
$Co(II)PCOOH^{-}$	Co(II)PCOOH	-1.1	-2.1	-1.0
$Co(II)PCOOH^{2-}$	$Co(II)PCOOH^{-}$	-2.1	NA	NA

Table 4. Redox potentials from quantum chemistry

Redox potential of various species using three functionals/computational methods, in volts. DFT+U results apply B3LYP vibrational and dielectric solvation contributions, but substitute B3LYP single-point energies with DFT+U ones.

and PAW pseudopotentials, setting U=2.5 eV yields binding energy for Eq. 13 that agree with experiments (see Ch. 2). Since neither CO_2 nor CO binds strongly to cobalt porphyrins at most accessible Co charge states, Eq. 13 yields the only binding constant in the literature available as a benchmark. While it is not guaranteed that this value of U is adequate for all Co charge states, fitting to Eq. 13 appears the most justifiable route to proceed.

Results

Redox potentials and hydration structures

The redox potential of the $A^{(n+1)-}/A^{n-}$ couple is the electron affinity (EA) of A^{n-} plus the difference in hydration free energies (ΔG_{hyd} of $A^{(n+1)-}$ and A^{n-}). Both EA and ΔG_{hyd} are readily obtained from quantum chemistry total energies that include approximate dielectric continuum solvation, zero point corrections, and finite temperature contributions. Taking the accepted value of 4.44 V as the standard hydrogen electrode half-cell potential, the redox values are listed in Table 4.

The Co charge state are assigned using maximally localized Wannier function analysis of AIMD aqueous phase simulation snapshots and may be slightly different from those in Ch. 2 which approximate the aqueous environment as a dielectric continuum. Here the DFT+U values are obtained by using B3LYP dielectric hydration and frequency information, but substituting single-point DFT+U energies for the B3LYP ones. DFT+U calculations, where available, show that B3LYP and DFT+U redox potentials track each other, while the PBE functional yields substantially different

results.

At first glance, B3LYP appears to predict a Co(I)P/Co(II)P redox couple value which disagrees with the average experimental value of -0.7 V (-0.6 to -0.8, depending on the porphyrin ring substituent and solvent). The redox potential also strongly depends on the DFT functional used, in contrast to the findings of Jaworska[8] for the Co(II)P-NO/$[Co(III)P\text{-}NO]^+$ system. While part of the discrepancy between B3LYP predictions and experimental redox potentials may be due to DFT inaccuracies, note that the DFT+U redox potential, fitted to Eq. 13, is also off by 0.8 volt. Thus uncertainties in the dielectric approximation used to calculate ΔG_{hyd} as well as the lack of ring substituents in our calculations may also be responsible. While PBE appears to yield a redox potential for the $[Co(I)P]^-$/Co(II)P couple similar to the experimental value, it performs worse in other cases, especially compared to DFT+U (see below).

To proceed, we focus on relative redox potential values and assume that all electrochemical measurements occur at the B3LYP $[Co(I)P]^-$/Co(II)P onset value (-1.7 V). The redox potential of other species relative to -1.7 V is then used to determine whether an additional electron has been incorporated in the intermediates. Thus, $[Co(I)P]^-$ and $[Co(II)PCOOH]^-$ are not reduced to $[Co(I)P]^{2-}$ and $[Co(II)PCOOH]^{2-}$, respectively, because the required voltages are more negative than -1.7 V. However, unlike $[Co(I)P]^-$ itself, $[Co(I)PCO_2]^-$ is already reduced to $[Co(I)PCO_2]^{2-}$ at -1.7 V. In other words, it is easier to add an electron to $[Co(I)PCO_2]^-$ in water than $[Co(I)P]^-$.

The reason can be qualitatively discerned in AIMD snapshots in explicit water (Fig. 3). Despite their net charges, both $[Co(I)P]^-$ and $[Co(I)P]^{2-}$ are effectively hydrophobic plates which do not form hydrogen bonds with water molecules. Neither does CO_2, a famously inert molecule. However, when they combine to form $[Co(I)PCO_2]^-$ or $[Co(I)PCO_2]^{2-}$, the resulting complex forms 4 to 5 hydrogen bonds with water through the partially negatively charged O atoms on the CO_2, which now adopt a bent geometry like a carbonate anion (Fig. 5c & d). This allows the ready accommodation of an extra electron. This effect can be significant not just for electrochemical reduction of CO_2, but for CO_2 capture on material substrates as well.

We also consider the hydration structures of Co(II)PCOOH and $[Co(II)PCOOH]^-$. The COOH group of the former complex readily donates a hydrogen bond to a H_2O molecule through its acid proton; this is faciliated by the fact that the C-OH "up" and "down" configurations are almost iso-energetic in the gas phase. In contrast, $[CoP(II)PCOOH]^-$ forms a strong intra-molecular hydrogen bond between the acid proton and one of the nitrogen atoms on the porphine ring. In the gas phase, this

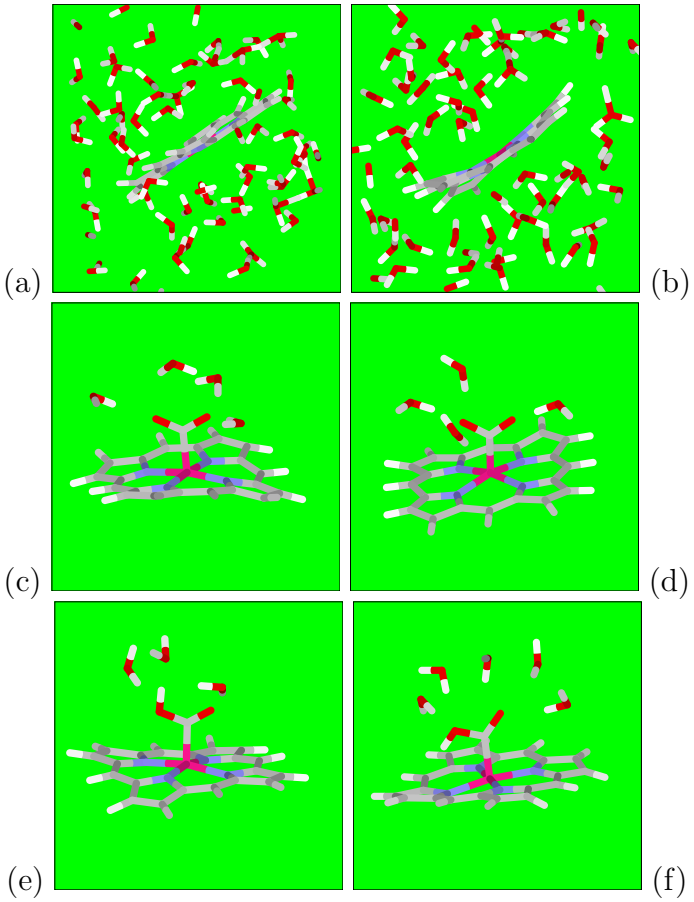

Figure 3. Snapshots of (a) $[Co(I)P]^{-}$; (b) $[Co(I)P]^{2-}$; (c) $[Co(I)PCO_2]^{-}$; (d) $[Co(I)PCO_2]^{2-}$; (e) Co(II)PCOOH; (f) $[Co(II)PCOOH]^{-}$; in water. In panels (c)-(f), most H_2O molecules are omitted; only those forming hydrogen bonds with the CoP structures are depicted. Panels (e) and (f) depict C-OH groups in the "up" and "down" configurations, respectively. The snapshots are taken after 1-2 ps AIMD trajectories. Pink sphere: Co; grey: C; red: O; white: H.

intramolecular hydrogen-bonded structure is 5 kcal/mol more stable than the configuration where the OH points upwards. This structure will feature prominently in the discussions below.

These redox potentials are consistent with an overall mechanism depicted in Fig. 4. The CO_2 addition and the first electron insertion steps are likely simultaneous. This is because while $[Co(I)P]^-$ should not be readily reduced to $[Co(I)P]^{2-}$, and CO_2 is not strongly bound to $[Co(I)P]^-$, the reaction

$$[Co(I)P]^{2-} + CO_2 \rightarrow [CoP(I)P - CO]_2^{2-}, \tag{14}$$

is very favorable—predicted to exhibit a significant binding free energy of 27 kcal/mol using the B3LYP functional, 6-31+G* basis set, and a dielectric treatment of the aqueous solvent. Even though the quantum chemistry calculations approximate water as a dielectric continuum, qualitative aspects of the hydration effect are evidently preserved. These energetics considerations support cooperative CO_2 and e^- addition. Indeed, if the CO_2 is thought of as part of the solvent, the electron transfer may be thought of as a solvent fluctuation-mediated process in a Marcus theory type of picture. Once the C-OH bond is severed to form a OH^-, the subsequent steps do not require further theoretical studies. This is because it is experimentally known that $[Co(I)P]^-$ and Co(II)P bind weakly to CO, and that these steps should be fast and non-rate-determining. It is possible that the two electron transfer steps themselves are rate-determining. However, such processes almost certainly will strongly depend on engineering aspects, e.g., the quality of the electrical contact between the catalyst and the gas-diffusion electrode. In contrast, the protonation and C-OH cleavage steps in Fig. 4 are at the heart of the catalytic function, and a deeper understanding of the scientific principles involved can lead to improved catalysts. In the next subsubsections, we consider these steps in detail using the AIMD method.

Deprotonation of $[CoPCOOH]^-$

We perform umbrella sampling AIMD simulations to calulate the potential of mean force ($W(R)$) of the following deprotonation reaction

$$[Co(II)PCOOH]^- \rightarrow [Co(II)PCOO]^{2-} + H^+. \tag{15}$$

Using water auto-ionization as a reference,[9] we estimate the pK_a of $[CoPCOOH]^-$ relative to the free energy of water-autoionization, assumed to exhibit pK_w=14. We apply a 4-atom reaction coordinate R=R_1-R_2-R_3,[10] where R_1, R_2 and R_3 are the distance between the oxygen atom on the proton-accepting H_2O and the COOH acid

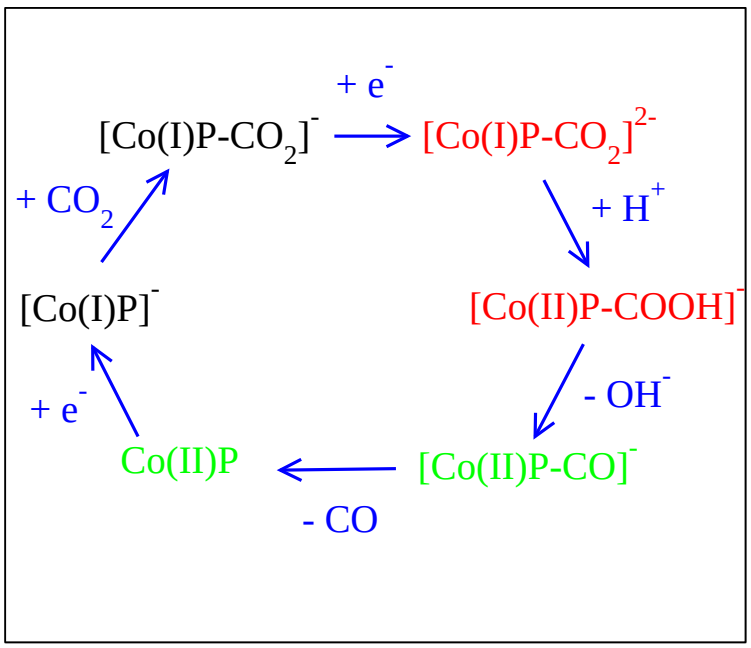

Figure 4. Mechanism of CO_2 reduction with electron addition. Red denotes key intermediates; green species should undergo fast reactions.

proton, and those between this O atom and the two protons originally belonging to the designated H_2O, respectively. $R > -0.7$ Å indicates an intact CO-H bond, while $R < -1.3$ Å is consistent with complete deprotonation.[10] Designating a special H_2O molecule can be done without loss of generality because all water molecules are interchangeable and only one is at any time close enough to the acid proton to be considered hydrogen bonded to it. In unconstrained AIMD trajectories, where umbrella sampling potentials are not applied, we find that the acid proton donates a hydrogen bond to water only 2% of the time. This hinders computational study of deprotonation, which can occur only if spontaneous fluctuations of the water configurations bring a H_2O molecule close enough to the acid proton. Our reaction coordinate and the umbrella constraining potentials conveniently ensures that hydrogen bond donation from the acid proton to water occurs during AIMD simulations.

Figure 5 depicts the deprotonation $W(R)$. Comparing the approximate bottom of the $W(R)$ well with that of water auto-ionization (assumed to exhibit pK_w=14.0), the pK_a of $[CoPCOOH]^-$ is estimated to be 9.0. Thus, $[Co(II)PCOOH]^-$ does not behave like an ordinary carboxylate acid with $pK_a \sim 4.5$. The significant reduction of acidity indicates that protonation of $[Co(I)CO_2]^{2-}$ is exothermic at the experimental conditions of pH > 7. In fact, as can be seen in Fig. 5, a minimum in $W(R)$ has not materialized. The true minimum should occur at larger values of the reaction coordinate R. The reason goes back to the fact that the acid proton does not readily donate a hydrogen bond to water; to attain this natural, non-hydrogen-bonding state, the H_2O molecule designated to accept a hydrogen bond from COOH must be displaced much further away. If an entropic correction is added to reflect this, the $[Co(II)PCOOH]^-$ pK_a would increase by at least one more pH unit. In contrast, a preliminary study of the deprotonation $W(R)$ of Co(II)PCOOH (Fig. 5) predicts a pK_a less than 4. Hence, adding an electron to the CO_2-ligated catalyst enhances its ability to hold on to excess protons. While this may appear obvious in retrospect, the specific atomistic mechanism of this rise in pK_a is intramolecular hydrogen bonding.

Comparison with the pK_a estimates of Ch. 2, which applies a dielectric continuum approximation for water molecules, is complicated by the strong DFT functional dependence (see Table 3 there). Our previous work on silica deprotonation suggests that B3LYP and PBE deprotonation free energies of simple OH groups should differ by only 1.1 kcal/mol, or less than 1 pH unit. Hence the large functional dependence of Ch. 2 is likely due to charge transfer between the COOH group and the Co ion, which would be much more sensitive to the choice of DFT functionals.

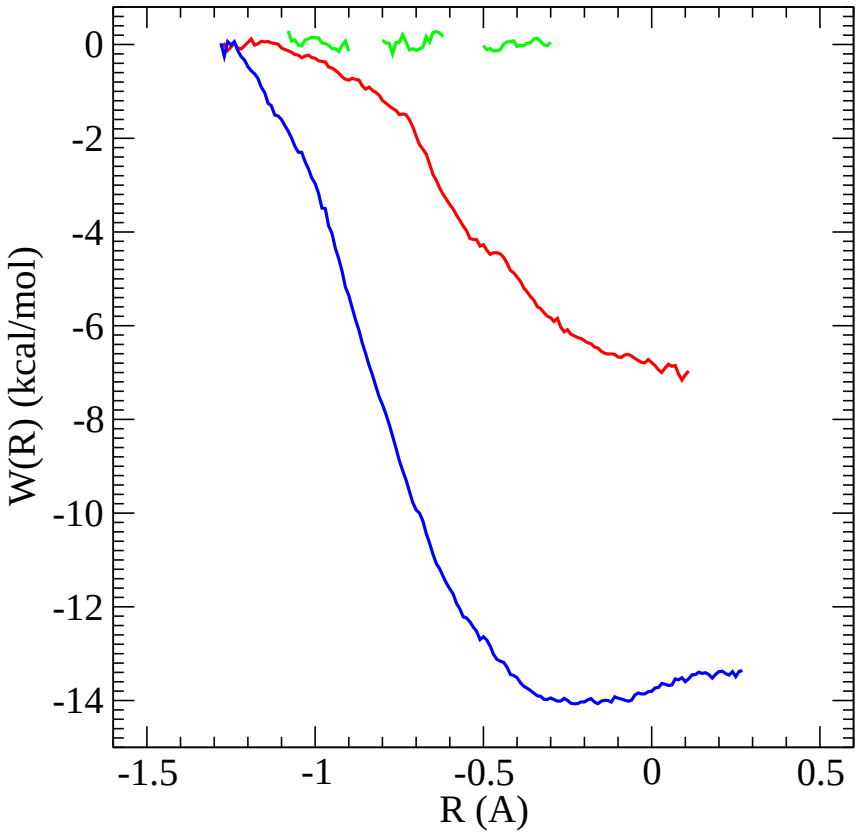

Figure 5. Red: $W(R)$ of $[\mathrm{Co(II)PCOOH}]^-$ deprotonation relative to that of water, depicted in blue and defined to be $\mathrm{pK_w}$=14. Green: preliminary deprotonation results for CoP(II)PCOOH, which exhibits a far stronger tendency towards deprotonation (i.e., higher acidity and lower $\mathrm{pK_a}$).

C-OH bond cleavage barrier

Using the C-OH bond distance as reaction coordinate, we next apply umbrella sampling to study the reaction

$$[\mathrm{Co(II)PCOOH}]^- \rightarrow [\mathrm{Co(II)PCO}] + \mathrm{OH}^-. \tag{16}$$

We use the C-O distance in this C-OH bond as the reaction coordinate. Figure 6a shows that this reaction is exothermic. The activation barrier is almost a factor of four smaller than that previously found for the uncatalyzed $CO_3H^- \rightarrow CO_2 + OH^-$ reaction.[11] Even though the comparison is not perfect, in that the carbon atom is not reduced to its +2 oxidation state in the previous work,[11] the cobalt porphyrin has clearly and drastically reduced the C-OH cleavage barrier. Unlike that previous work,[11] we have not constrained the OH bond rotation around the C-O axis and then corrected for the entropic contributions there. This is because the PBE functional we use is consistent with much faster OH^- dynamics in water than the RPBE functional previously applied;[11, 12, 13] thus the OH rotation around the C-O axis can be assumed to be well-sampled within the 10 ps AIMD trajectories.

After accounting for standard state and entropy corrections, we obtain a free energy of reaction ΔG = -6.0 kcal/mol and a barrier height ΔG^* = 5.2 kcal/mol. Zero point energy corrections have not been included but should not exceed 2 kcal/mol. This calculation thus confirms that the reaction is exothermic, and, as already discussed above, the activation free energy is fairly low. Note that, although the free energy change does not depend on the reaction coordinate, the activation barrier does vary with the reaction coordinate chosen. A more systematic approach may be to use the path-sampling method,[14] which is however computationally costly. Instead, as in our previous work,[11], we have computed the transmission coefficient κ[15] by randomly taking 10 configurations and velocities at the top of the barrier as initial conditions, restart AIMD trajectories without umbrella sampling constraints, and record whether any recrossing of the barrier is observed in these 10 trial runs. We find that $\kappa = 0.6$, which indicates that R_{CO} is a reasonable reaction coordinate. This suggests that our reported ΔG^* should be reliable.

Unlike Ch. 2, we have focused on Eq. 16 and not the proton-assisted variation

$$\begin{aligned} [\mathrm{Co(II)PCOOH}]^- + \mathrm{H}^+ &\rightarrow \mathrm{Co(II)PCO - OH_2}; \\ \mathrm{Co(II)PCO - OH_2} &\rightarrow [\mathrm{Co(II)PCO}] + \mathrm{H_2O}. \end{aligned} \tag{17}$$

Thermodynamically the two are equivalent, but kinetically they will have different activation barriers. To estimate ΔG^* for Eq. 17, we note that AIMD $W(R)$ calculated

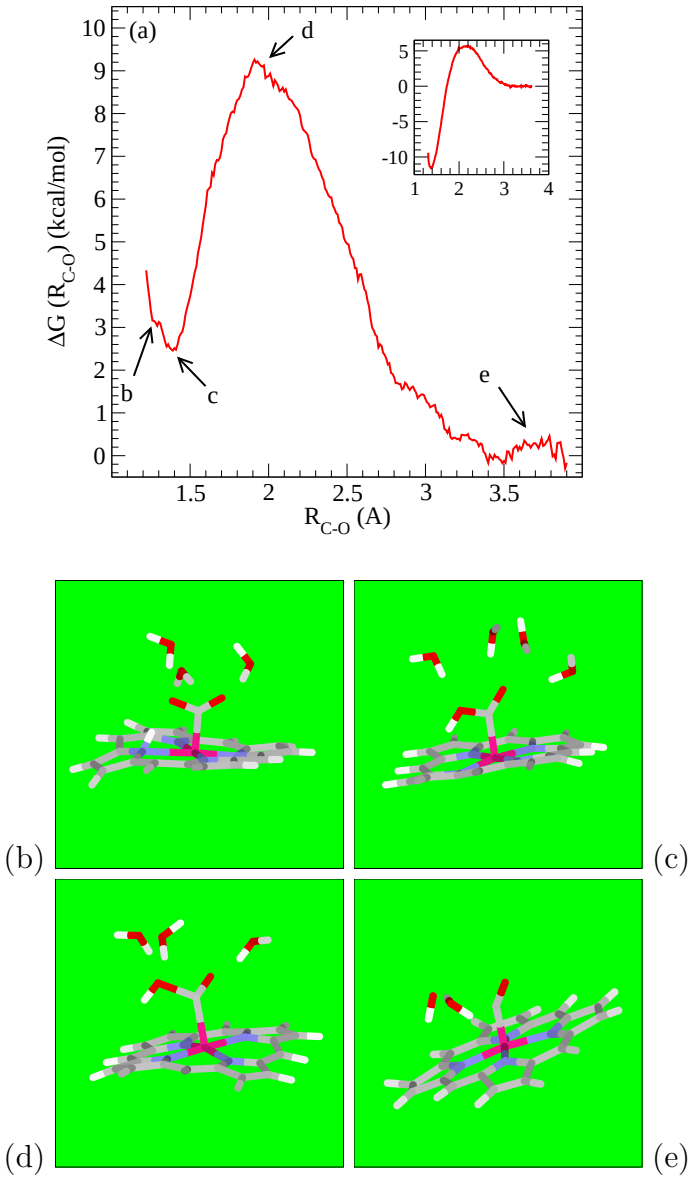

Figure 6. (a) $W(R)$ for the C-OH cleavage reaction, Eq. 16. Inset: $W(R)$ for $CO_3H^- \rightarrow CO_2 + OH^-$.[11] (b)-(d): snapshots in the four umbrella sampling windows indicated in panel (a). The AIMD simulations are performed in an explicit liquid water environment; only a few water molecules are shown in these snapshots.

for all protonation/deprotonation reactions examined in the literature are invariably monotonic, i.e., the free energy changes and activation barriers are the same. Assuming the second half of Eq. 17 is also barrierless, ΔG^* for Eq. 17 would be entirely due to the ΔG of the first half of Eq. 17, namely, the pK_a of $Co(II)PCOOH_2$. At pH=8, the pK_a of the C-OH_2 group in $Co(II)PCOOH_2$ will have to exceed 4.2 in order to yield a barrier lower than the $\Delta G^* = 5.2$ kcal/mol we find for Eq. 16. This appears extremely unlikely. In the future, we plan to explicitly model the deprotonation reaction associated with Eq. 17.

Conclusions

In this chapter, we have extracted redox potentials from quantum chemistry calculations using the B3LYP functional. Even though the absolute value for the $[Co(I)P]^-/Co(II)P$ couple is not in good agreement with experiments, the relative values of various redox potentials allow us to determine where the electron transfers occur among the four intermediate steps. Due to their enhanced interaction with water compared to $Co(I)P^-$, $[Co(I)PCO_2]^{2-}$ and $[Co(II)PCOOH]^-$ are the key intermediates. This finding may be useful for not just electrochemical reduction of CO_2, but for CO_2 capture from flue gas and even the atmosphere. These intermediates appear consistent with quantum chemistry predictions reported in Ch. 2

AIMD umbrella sampling calculations show that the pK_a associated with $[Co(II)PCOOH]^-$ deprotonation is at least 9.0. This indicates that the protonation of $[Co(I)PCO_2]^{2-}$ is exothermic and downhill at the predominant experimental conditions (bicarbonate buffer, pH $\sim$7 to 8). The subsequent cleavage of the C-OH bond is also exothermic, and the activation free energy involved is only 5.2 kcal/mol. If we assume a vibrational pre-factor of k=0.1 ps^{-1}, the time scale of C-OH cleavage would be nanoseconds at T=300 K. Thus this reaction should proceed readily.

References

[1] Kresse, G.; Furthmüller, J. *Phys. Rev. B* **1996**, *54*, 11169; *Comput. Mater. Sci.* **1996**, *6*, 15.

[2] Kresse, G.; Joubert, D. *Phys. Rev. B* **1999**, *59*, 1758.

[3] Perdew J. P.; Burke K.; Ernzerhof M. *Phys. Rev. Lett.* **1996**, *77*, 3865.

[4] Schwegler, E.; Grossman, J.C.; Gygi, F.; Galli, G. *J. Chem. Phys.* **2004**, *121*, 5400; Sit, P.H.-L.; Marzari, N. *J. Chem. Phys.* **2005**, *122*, 204510; Rempe, S.B.; Mattsson, T.R.; Leung, K. *Phys. Chem. Chem. Phys.* **2008**, *10*, 4685.

[5] Anisimov, V. I.; Zaanen, J.; Andersen, O. K. *Phys. Rev. B*, **1991**, *44*, 943; Liechtenstein, A. I.; Anisimov, A. I.; Zaanen, J. *Phys. Rev. B* **1995**, *52*, 5467.

[6] Leung, K.; Rempe, S.B.; Schultz, P.A.; Sproviero, E.M.; Batista, V.S.; Chandross, M.E.; Medforth, C.J. *J. Am. Chem. Soc.* **2006**, *128*, 3659.

[7] Leung, K.; Medforth, C.J. *J. Chem. Phys.* **2007**, *126*, 024501.

[8] Jaworska, M. *Chem. Phys.* **2007**, *332*, 203.

[9] Ivanov, I.; Chen, B.; Raugei, S.; Klein, M.L. *J. Phys. Chem. B* **2006**, *110*, 6365.

[10] Leung, K.; Nielsen, I.M.B.; Criscenti, L.J. (unpublished).

[11] Leung, K.; Nielsen, I.M.B.; Criscenti, L.J. *J. Phys. Chem. B* **2007**, *111*, 4453.

[12] Hammer B.; Hansen L. B.; Norskov J. K. *Phys. Rev. B* **1999**, *59*, 7413.

[13] Asthagiri D.; Pratt L. R.; Kress J. D.; Gomez M. A. *Proc. Natl. Acad. Sci.* **2004**, *101*, 7229; Tuckerman M. E.; Marx D.; Parrinello M.; *Nature* **2002**, *417*, 925; Tuckerman M. E; Chandra A.; Marx D. *Acc. Chem. Res.* **2006**, *39*, 151.

[14] Geissler, P.L.; Dellago, C.; Chandler, D.; Hutter, J.; Parrinello, M. *Science*, **2001**, *291*, 2121.

[15] See, for example, Chandler D. *Introduction to Modern Statistical Mechanics*, Oxford University Press, New York, 1987.

4 Electronic structure methods

In this chapter, we briefly describe our progress towards the improvement of electronic structure theory for predicting the catalytic and optoelectronic properties of first row transition metal ion complexes and oxides.

Quasi-self-interaction correction

In collaboration with Nicola Spaldin's research group at the University of Santa Barbara, we initially planned to explore using the quasi-self-interaction-correction (q-SIC) method to model cobalt porphyrin catalysts. As the project proceeded, the Spaldin group made discoveries that prompted them to move away from this technique.[1] However, a recent advance in her group, which involves implementing a finite electric field in condensed matter (either solid or liquid) settings,[2] may be extremely useful for calculations pertaining to electrochemical reactions. This is an area we will explore in the future.

Self-consistent DFT+U

In collaboration with Nicola Marzari's research group and graduate student Heather Kulik at MIT, we have pursued using a self-consistent DFT+U technique to determine the values of U in different molecular configurations. This method applies a linear-response procedure to calculate U instead of parameterizing U to yield experimentally observed binding energies, as was done in Ch. 3. The reaction intermediates are predicted to exhibit U values between 5 and 7 eV when using atomic orbitals implemented in the Quantum Expresso code to project d-orbital occupancies required in DFT+U calculations. Adopting an average value of U=6 eV, the predicted binding energies and spin states of cobalt porphine-carbon monoxide complexes are listed in Table 5.

The binding energy for the benchmark $[Co(III)P\text{-}CO]^+$ complex is superficially similar to that calculated with the B3LYP functional (see Ch. 2). However, this reported value has not yet included the change in spin states. Specifically, it measures the energy difference between low-spin $Co(III)P^+ + CO$ and low-spin $[Co(III)P\text{-}CO]^+$, but the stable high-spin $[Co(III)P^+]$ is more appropriate to the thermodynamic cycle reported in the experimental work. Further work on evaluating this binding energy is currently under way. A separate, detailed report on Heather Kulik's work is avail-

species	E_{bind} (eV)	spin (μ_B)
CoP-CO^-	0.64	0.00
CoP-$CO_2{}^-$	0.10	0.00
CoP-CO	0.06	1.00
CoP-CO_2	unbound	NA
CoP-CO^+	0.24	0.00
CoP-CO^+	0.04	0.00

Table 5. Binding energies and spin states of various CoP-CO complexes.

able in pdf format upon request. Self-consistent evaluation of U is a new research area, and recent developments suggest that the current implementation may be further improved upon in the near future.[5, 6] Even the existing, empirical U-value DFT+U approach has proven reliable when predicting lithium ion battery cathode oxide properties while semi-local functionals has demonstrated notable failures in band gaps and in the phase diagram.[7] Thus, the electronic structure methods explored in this LDRD are also critical for modeling electricial energy storage processes as well.

Semi-local functionals

Non-hybrid, semi-local DFT functionals often yield very similar predictions for transition metal complexes.[10, 11] We have explored various semi-local exchange correlation functionals in the absence of "+U" augmentation.[8, 9] Instead of using cobalt porphyrins as test cases, we have considered the electronic band gap and magnetic moments of transition metal oxides as efficient collective benchmarks. Indeed, these were the first benchmarks chosen by Liechtenstein *et al.* in their pioneering paper on DFT+U calculations.[12]

Figure 7 depicts the electronic densities of state (DOS) and magnetic moments per unit cell of CuO computed using different functionals. As can be seen, pure DFT functionals (i.e., $U = 0$ eV) predict metallic behavior and zero magnetic moments, whereas the use of a large $U = 7.5$ eV value correctly predicts insulating behavior and a finite magnetic moment. Such behavior is prevalent for the first row transition metal oxides.[12] Non-hybrid functionals not augmented with "+U" methods typically yield band gaps which are factors of 20 or more smaller than experimental values,[12] they

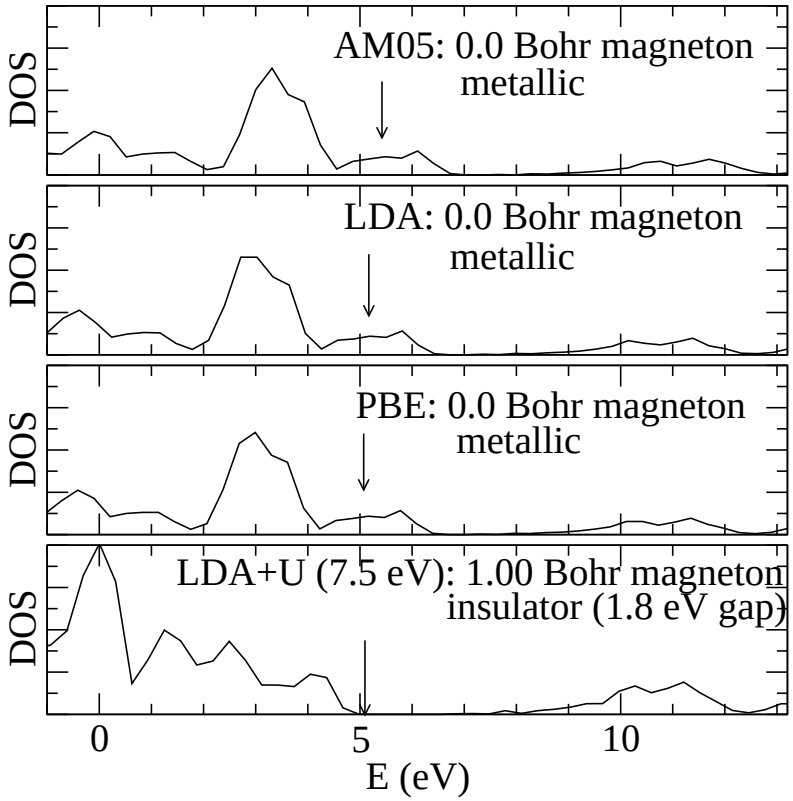

Figure 7. Kohn-Sham densities of state for CuO computed using various electronic structure methods. For simplicity, a ferromagnetic ordering is imposed on the LDA+U CuO structure.

have also been known to yield zero gap metallic states when the experimental gaps exceed 3 eV![7, 12]

We stress that, even in semiconducting systems like bulk silicon which do not contain partially filled *d*-orbital elements, non-hybrid functionals underestimate the band gap by $\sim 40\%$ or more. This has been attributed to the lack of discontinuity in the exchange-correlation functional. What is specific to the first row transition metal oxides is that their band gaps are underestimated by at least an order of magnitude, which seldom occurs in main group insulators—unless DFT treatment of the latter (like Ge solid) is close to a metal-insulator transition. (Here we should stress that transition metal oxides undergo charge-transfer or Mott-Hubbard metal insulator transitions, while the transition in Ge is of the Wilson band-crossing type; the mechanisms are very different.)

Transition metal oxides are special because *another* source of error is at work in these materials, namely the extremely poor treatment of strongly localized *d*-orbital electrons within most semi-local functionals. This error is largely absent in silicon or diamond. *Thus it is incorrect to attribute the band gap errors in both cases to functional discontinuities.* An automobile that fails to start may have a broken-down starter coil, but alternatively its battery may have run down. Another fallacy is to claim that the Kohn-Sham single electron states have no physical meaning whatsoever. Empirically, it is well known that TDLDA calculations in the adiabatic approximation yield onsets of optical absorption spectra (physical, measurable properties) which are very similar to the magnitude of the Kohn-Sham band gap. Asserting that the Kohn-Sham gap has no physical meaning is also clearly untenable near the metal-insulator transition, where a system with no band gap in the Kohn-Sham single-electron density of state invariably yields a diverging static dielectric constant (i.e., metallic behavior). As semi-local functionals often erroneously predict zero gaps in transition metal oxides which are in reality insulators, these functionals necessarily exhibit fundamental errors in the ground state properties of transition metal oxides.

Note that a recent semi-local functional, with parameters fitted to a database, has shown promising thermochemical predictions for transition metal complexes, and raises the hope that accurate AIMD simulations with cost-efficient non-hybrid functionals can be performed without the "+U" augmentation in the future.[13]

Other methods

Another much heralded technique used to deal with strongly-correlated electron systems, including the various phases of plutonium metal, is the Dynamical Mean Field Theory (DMFT) method.[14] However, forces on atoms are apparently not easily computed therein, and DMFT-based molecular dynamics seem out of the question. Nevertheless, a recent development, which approximates DMFT electronic states with Gutzwiller wavefunctions, seems very promising. It will likely yield predictions more accurate than fixed U value DFT+U at a similar computational cost, potentially enabling large scale AIMD simulations. We will explore this approach in the future in the context of f-electron (actinide) systems pertinent to a new-start nuclear energy LDRD.

References

[1] Stengel, M.; Spaldin, N.A. *Phys. Rev. B* **2008**, *77*, 155106.

[2] Stengel, M.; Spaldin, N.A. *Phys. Rev. B* **2007**, *75*, 205121.

[3] Cococcioni, M.; de Gironcoli, S. *Phys. Rev. B* **2005**, *71*, 035105.

[4] Kulik, H.J.; Cococcioni, M.; Scherlis, D.A.; Marzari, N. *Phys. Rev. Lett.* **2006**, *97*, 103001; Kulik, H.J., Marzari, N. *J. Chem. Phys.* **2008**, 129, 134314.

[5] Campo, V.L.; Cococcioni, M. `http://arXiv.org/abs/0907.5272v2`.

[6] Zhou, F.; Ozolins, V. `http://arXiv.org/abs/0907.2700v1`.

[7] Zhou, F.; Marianetti, C.A.; Cococcioni, M.; Morgan, D.; Ceder, G. *Phys. Rev. B* **2004**, *69*, 201101.

[8] Armiento, R.; Mattsson, A.E. *Phys. Rev. B* **2005**, *72*, 085108.

[9] Perdew, J.P.; Burke, K.; Ernzerhof, M. *Phys. Rev. Lett.* **2006**, *77*, 3865.

[10] Reiher, M.; Salomon, O.; Hess, B. A. *Theor. Chem. Acc.* **2001**, *107*, 48.

[11] Reiher, M. *Inorg. Chem.* **2002**, *41*, 6928.

[12] Liechtenstein, A. I.; Anisimov, A. I.; Zaanen, J. *Phys. Rev. B* **1995**, *52*, 5467.

[13] Zhao, Y.; Truhlar, D.G. *J. Chem. Phys.* **2006**, *125*, 194101.

[14] Kotliar, G.; Savrasov, S.Y.; Haule, K.; Oudovenko, V.S.; Parcollet, O.; Marianetti, C.A. *Rev. Mod. Phys.* **2006**, *78*, 865.

[15] Wang, G.T.; Dai, X.; Fang, Z. *Phys. Rev. Lett.* **2008**, *101*, 066403.

DISTRIBUTION:

1	MS 1415	Kevin Leung, 1114
1	MS 1415	Ida M.B. Nielsen, 8961
1	MS 0745	John A. Shelnutt, 1815
1	MS 1415	Carlos Gutierrez, 1114
1	MS 0888	Regan W. Stinnet, 1821
1	MS 0734	Ellen B. Stechel, 6339
1	MS 0754	Patrick V. Brady, 6310
1	MS 0734	Chad L. Staiger, 6338
1	MS 0734	Timothy N. Lambert, 6339
1	MS 9536	Technical Library, 0899 (electronic copy)
1	MS 0123	D.L. Chavez, 1011